NTNU
Norwegian University of
Science and Technology

Low Frequency Alternating Current (LFAC) Transmission Systems for Offshore Wind Farms

Case Studies on the Use of LFAC, Based on
Horns Rev 3 Offshore Wind Farm

Kim Allgot

Master of Energy and Environmental Engineering
Submission date: June 2017
Supervisor: Elisabetta Tedeschi, IEL
Co-supervisor: Santiago Sanchez Acevedo, IEL

Norwegian University of Science and Technology
Department of Electric Power Engineering

Low Frequency Alternating Current (LFAC) Transmission Systems for Offshore Wind Farms

- Case Studies on the Use of LFAC, Based on *Horns Rev 3* Offshore Wind Farm

Kim Allgot

June, 2017

Preface

This thesis is the result of my 11$^{\text{th}}$ and final semester as a full-time student at the *Department of Electric Power Engineering*, *NTNU*.

Esa Virtanen, vice president of Technology and Engineering from *ABB Oy Transformers* in Finland has provided the thesis with valuable input regarding low frequency operation of several components central to the power system, such as transformers and reactors. The input has been much appreciated and I thank him for his support.

Valuable information about the actual topology and operation of *Horns Rev 3* was provided by *Energinet* in Denmark, and I would like to express my gratitude to Søren Juul Larsen and Christian Flytkjær Jensen.

The main supervisor for this master thesis has been Professor Elisabetta Tedeschi. I would like to express my sincere gratitude to her for being enthusiastic and supportive, and finding the time to give valuable feedback throughout the process of writing this thesis, despite her busy schedule.

Additional support has been given by Santiago Sanchez Acevedo, who has been the co-supervisor for this thesis. I would like to thank him for the support in building the simulation model and providing valuable ideas and feedback throughout the work on this thesis.

Lastly, I would like to thank all those who stood by my side through my seven years as a student. To the city of Trondheim, the university and for all the exciting opportunities I have been given these past seven years. I have learned a lot from many great men and women, and I am really looking forward to apply my knowledge in a context outside of *NTNU*.

NTNU, Trondheim, June 2017

Kim Allgot

Abstract

This thesis investigates the use of low frequency alternating current (LFAC) for the long-distance transmission of the power extracted from offshore wind farms. It is based on the measurement of power flow in different nodes in the system simulating an offshore wind farm being built outside the coast of Denmark, *Horns Rev 3 (HR3)* . The results for scenarios simulating different lengths of the offshore cable and the operating frequency of the system are compared. Reactive power compensation is used to improve the power flow of the system and to counteract the reactive current from the capacitance in the long offshore cable.

Power flow, voltage- and current limitations of the offshore cable, and varying the reactive power compensation in the different nodes are used to assess if the different scenarios described are feasible or not. Considerations related to size and operation at reduced frequency on the different power system components are mentioned and discussed briefly. The thesis does not include any detailed analysis with regards to a possible increase in cost for the different components operating at reduced frequency.

The thesis concludes that the use of LFAC gives reductions regarding power losses, improving the power system efficiency. For the real case of *HR3*, using LFAC excludes the need for reactive power compensation. The thesis also proves that it is possible to transmit substantial amounts of power over longer distances than any other AC-cable in operation today. It is proved that using LFAC and reactive power compensation from shore, it is possible to transmit over 370 MW to the grid with an overall efficiency of more than 93 %, at a distance of 200 km using a 220 kV offshore cable. Including reactive power compensation from the offshore end of the cable, the distance can be increased to 300 km, delivering over 370 MW of power to the grid with an overall efficiency of 91 %.

However, the weight and size of LFAC transformers are considerably higher than the equivalent 50-Hz components, with up to 2.7 times the weight, this would be a challenge for the construction of the offshore substation transformers.

Beyond the scope of this thesis further investigations are needed regarding costs for the different components of the system, as this is not included.

Sammendrag

Denne oppgaven omhandler bruk av lavfrekvent kraftoverføring ved bruk av vekselstrøm (eng. low frequency alternating current, LFAC) for lange overføringskabler fra vindkraftparker offshore. Oppgaven er basert på målinger av kraftflyt gjennom ulike noder i systemet, som er simulert med utgangspunkt i en offshore vindkraftpark som er under bygging utenfor kysten av Danmark, *Horns Rev 3*. Resultatene for scenarioene med ulik kabellengde og nettfrekvens er sammenliknet med hverandre. Reaktiv kompensering er benyttet for å bedre kraftflyten i systemet og for å motvirke den reaktive strømmen fra de kapasitive elementene i den lange offshorekabelen.

For de ulike scenarioene kan man ved å variere den reaktive kompensasjonen i de ulike nodene undersøke kraftflyten, samt om systemet opererer innen de maksimale begrensningene i offshorekabelen for maksimal spenningspåkjenning og strøm. Betraktninger knyttet til vekt og størrelse for de ulike bestanddelene i kraftsystemet ved redusert frekvens er omtalt. Oppgaven inkluderer ikke noen detaljert analyse med tanke på eventuelle økte kostnader for de ulike bestanddelene når de opererer under redusert frekvens.

Oppgaven konkluderer med at lavfrekvent kraftoverføring fører til reduserte effekttap og gjennom dette en høyere virkningsgrad for kraftsystemet. Det reelle scanarioet for *Horns Rev 3* vil ikke ha behov for reaktiv kompensering ved bruk av den foreslåtte reduserte frekvensen (16.7 Hz) i kraftsystemet. Oppgaven viser at det er mulig å transportere store mengder effekt over lengre distanser enn noen andre vekselstrømskabler som i dag er i drift. Det er vist at det er mulig ved bruk av lavfrekvent kraftoverføring og reaktiv kompensering fra land, å overføre mer enn 370 MW til sentralnettet, med en total virkningsgrad på over 93 %, en distanse på 200 km gjennom en 220 kV offshorekabel. Ved bruk av reaktiv kompensering fra begge ender av kabelen, kan avstanden økes til 300 km og overføre 370 MW til sentralnettet med en virkningsgrad på 91 %.

Både størrelse og vekt for de lavfrekvente transformatorene er betydelig høyere enn for de tilsvarende 50-Hz utgavene, med en vekt som er opptil 2.7 ganger så stor. Dette vil være en utfordring ved bygging av transformatorstasjonen offshore.

I tillegg til hva som har blitt undersøkt i denne oppgaven er det ytterligere behov for undersøkelser og analyser med tanke på kostnadene for de ulike komponentene i et lavfrekvent kraftsystem.

Contents

List of Figures

List of Tables

Abbreviations

AC	**A**lternating **C**urrent
CSP	**C**onsentrated **S**olar **P**ower
DC	**D**irect **C**urrent
EMF	**E**lectro**m**otive **F**orce
GIS	**G**as **I**nsulated **S**witchgear
HV	**H**igh **V**oltage
IEA	**I**nternational **E**nergy **A**gency
IEC	**I**nternational **E**lectrotechnical **C**ommision
LFAC	**L**ow **F**requency **A**lternating **C**urrent
LV	**L**ow **V**oltage
MATLAB	**Mat**rix **Lab**oratory (computer software)
OECD	The **O**rganization for **E**conomic **C**o-operation and **D**evelopment
OWF	**O**ffshore **W**ind **F**arm
POC	**P**oint **o**f **C**onnection
PLL	**P**hase-**L**ocked **L**oop
PV	**P**hoto-**V**oltaic
PI controller	**P**roportional **I**ntegral controller
PM	**P**ermanent **M**agnet

RMS	**R**oot **M**ean **S**quare
STE	**S**olar **T**hermal **E**nergy
TSO	**T**ransmission **S**ystem **O**perator
WTG	**W**ind **T**urbine **G**enerator
XLPE	Cross-**L**inked **P**oly**E**thylene

Symbols

P	Active power	pu or Watt (W)
ρ	Air density	kg/m^3
Al	Aluminium	
ω	Angular frequency	$\frac{\text{rad}}{s}$
S	Apparent power	pu or Volt-Ampere (VA)
A	Area	m^2
β	Blade pitch angle	rad or deg.
C	Capacitance	pu or Farad (F)
Cu	Copper	
I	Current	pu or Ampere (A)
η	Efficiency	%
f	Frequency	pu or Hertz (Hz)
j	Imaginary unit	
L	Inductance	pu or Henry (H)
$\mathbf{H}$	Magnetic field	Ampere per meter, $\text{A} \cdot \text{m}^{-1}$
Φ_B	Magnetic flux	Weber (Wb)
$\mathbf{B}$	Magnetic flux density	Tesla (T)
μ	Magnetic permeability	H/m

$\mathbf{M}$	Magnetic polarization	
N	Number of turns	
pu	Per unit	
$\cos\phi$	Power factor	pu
C_p	Power coefficient	pu
γ	Propagation constant	
X	Reactance	pu or Ohm (Ω)
Q	Reactive power	pu or Volt-Ampere Reactive (Var)
R	Resistance	pu or Ohm (Ω)
δ_S, δ_R	Sending and receiving end voltage angle	rad or deg.
λ	Tip speed ratio	pu
V	Voltage	pu or Volt (V)
U	Wind speed	m/s

Chapter 1

Introduction

The demand for energy continues to increase. To get people out of poverty, the world needs energy that doesn't rely solely on fossil fuels. Renewable energy from geothermal, solar (both Photo-Voltaic (PV) and thermal), hydro and wind is important in order to reach the goals for energy. The world population continues to grow and predictions from the *United Nations* estimates that the population will increase from approximately 7.35 billion people in 2015, to over 9.7 billion people in 2050 [1], an increase of more than 32 %.

The frightening backdrop of global warming, rise of the sea-level, melting of the polar ice etcetera and the increasing global CO_2-emissions forces innovative solutions to be made with regards to how we supply an increasing population with energy. To achieve our sustainability goals we have come to realize that much of the new energy solutions must be based on renewable energy. To this backdrop, the importance of generating electric power from wind energy presents itself as a promising and important contribution.

The growth of energy delivered by wind power has increased tremendously over the last two decades as the technology have matured and the costs have gone down. Every single year from 1995-2012, the global annual growth has been more than 17 %, as shown in figure 1.0.1. The *Technology Roadmap, Wind Energy, 2013* by *IEA/OECD* [2] states that since 2008, total wind power deployment has more than doubled, approaching 300 GW (including both on- and offshore) and now provides 2.5 % of global electricity demand. The roadmap also targets 15 % to 18 % of global electricity to come from wind power by 2050. In 2050 the total 2 300 GW to 2 800 GW of installed wind capacity (on- and

offshore) will avoid emissions of up to 4.6 gigatons of carbon dioxide (CO_2) globally per year. The roadmap predicts the cost of energy from wind to decrease by up to 25 % for onshore and 45 % for offshore installations by 2050, compared to 2013 costs.

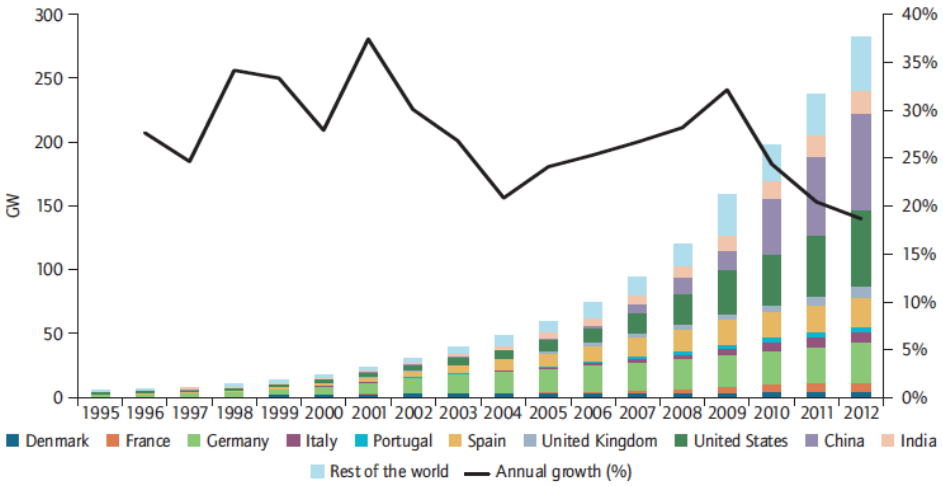

Figure 1.0.1: Global cumulative growth of wind power capacity, 1995-2012 [2]

Due to public opposition to onshore wind farms due to the use of area, visual pollution and acoustic noise there is suggested that more wind farms should be placed offshore. This reveals new technical challenges that needs to be solved before offshore wind farms can be developed in a larger scale.

The offshore wind farms (OWFs) constructed today are placed in shallow waters on depths of up to 50 metres. These structures are fastened at the sea-bottom using either monopile constructions, jackets or tripods. For depths of more than 50 meters there is need for floating wind turbines, and the first full scale pilot *Hywind* was installed in 2009 at 200 meters depth, outside of Karmøy, Norway, with a capacity of 2.3 MW. The pilot has been a success and the turbine produced 10.1 GWh of energy in 2011, giving a capacity factor of more than 50 %. In 2015 Statoil applied for moving the turbine from the location outside of Karmøy to the oil platform *Valemon*, located 120 km off the western coast of Norway. There it was intended to be used to decrease the use of gas turbines at the platform, and *Statoil* estimated that the reductions in CO_2 emissions could be as high as 11 000 tons per year [3]. The plan to move the turbine was supported by *The Norwegian Water Resources and Energy Directorate (NVE)* [4]. The plans were later abandoned by *Statoil* because of lower estimates for the number of days the gas-turbine at *Valemon* could be turned off using the power from the turbine, compared to what was originally calculated [5]. Due to the success of the first pilot *Statoil* is now planning to

build an offshore wind pilot park 25 km off the coast of Scotland, consisting of five 6 MW floating turbines. The plan is that the park is to be commissioned in 2017 [6].

According to the *International Energy Agency (IEA)*, energy generation from offshore wind in the *OECD*-countries [7] was in 2015 projected to increase from 25 TWh in 2014 to 76 TWh in 2020. In their most recent report, the *IEA Medium-Term Renewable Energy Market Report 2016*, shows that the annual global electricity generation from offshore wind is expected to increase from 25 TWh in 2014 to approximately 110 TWh in 2021. Figure 1.0.2 show the predicted annual capacity additions and the energy production from offshore wind from 2014-2021.

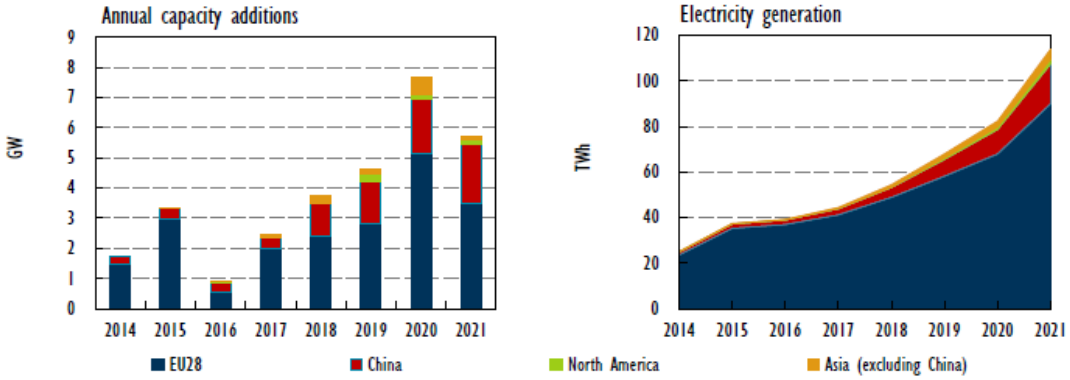

Figure 1.0.2: Annual capacity additions (GW) and Electricity generation (TWh), 2014-2021 [8]

The installed offshore wind power capacity in Europe was, according to the *International Renewable Energy Agency (IRENA)*, reported at over 12.4 GW at the end of 2016 [9]. Globally the offshore installed wind capacity was projected to reach 28.8 GW in 2020 as reported by IEA *Medium-Term Renewable Energy Market Report 2015* [7], but the newest report, from 2016 has adjusted this prediction to 31.4 GW in 2020 and 36.3 GW in 2021, as shown in table 1.0.1. For their accelerated case, as much as 43 GW is expected in 2021 [8].

However, if the wind farms are to be located far offshore there are issues regarding power transmission.

[1] **C**onsentrated **S**olar **P**ower, **S**olar **T**hermal **Energy**

Table 1.0.1: World renewable electricity capacity forecast, main and accelerated cases (GW) [8]

	2015	**2016**	**2017**	**2018**	**2019**	**2020**	**2021**	**2021 Accelerated**
Hydropower	1 205	1 232	1 258	1 283	1 305	1 324	1 340	1 369
Bioenergy	105	110	116	122	129	134	140	159
Wind	417	468	517	568	621	683	740	815
Onshore	405	455	502	548	598	652	703	772
Offshore	**12**	**13**	**16**	**19**	**24**	**31**	**36**	**43**
Solar PV	225	288	338	386	438	492	547	654
CSP/STE[1]	5	5	6	7	8	10	11	15
Geothermal	13	13	14	14	15	16	17	18
Ocean	1	1	1	1	1	1	1	1
Total	**1 969**	**2 117**	**2 251**	**2 382**	**2 518**	**2 660**	**2 795**	**3 031**

1.1 Problem Background and Motivation

To evacuate power from offshore wind farms to shore it is possible to export the power using alternating current (AC) transmission as generated from the turbines using step up transformers and, if needed, reactive power compensation. Or it is possible to use an offshore converter to rectify the AC current from the generators into direct current (DC) before transmitting DC power onshore. However, there are drawbacks with both options and the motivation for doing this thesis is to investigate if there is some sort of middle ground between the two solutions, by using a lower operating frequency for the AC-system.

1.1.1 Martin Linge, World's Longest AC-cable

The longest AC-link in the world is the 164 km long 100 kV AC-cable supplying 55 MW to the offshore platform *Martin Linge* in the *North Sea*. There is only reactive power compensation from the onshore side of the cable [10].

1.2 Limitations of Scope

The objective of this thesis is to investigate how frequency influences reactive power regarding evacuation of power from offshore wind farms. It also simulates the different components in the power system and describes their behavior regarding a change in frequency from the normal frequency of 50 or 60 Hz. The analysis will be done in steady state and there are no dynamic/transient investigations included in this thesis. The case used as a backdrop for this thesis is the construction of *Horns Rev 3 Offshore Wind Farm* outside of Denmark by *Vattenfall AB*. The actual wind farm will include inter-array cables, but to limit the scope of this thesis the 49 turbines are aggregated delivering power to the three substation transformers without the 33 kV inter-array cables. The back-to-back onshore converter converting the frequency from 16.7 Hz to 50 Hz is not simulated.

The aspects regarding costs of the different components are not described in detail. Hence the thesis investigates whether it is technically possible to make the topologies suggested, while decisions to build or not will rest upon an analysis of the costs and benefits of each specific project.

1.3 Relation to Specialization Project

The author wrote a specialization project at the *Norwegian University of Science and Technology* in the autumn of 2015 titled *Low Frequency AC Transmission for Offshore Wind Farms* [11]. The objective of the project was to investigate whether reducing the frequency of an AC grid seemed a viable solution for evacuating power from offshore installations at mid-range distances from shore. The project was conducted as a literature study where fundamental circuit analysis as well as Faradays laws and electromagnetic theory was used to describe the basis for reduced frequency operation of both generators, transformers and cables. This was supported by an extensive investigation of relevant updated research papers considering different aspects of frequency dependent parameters in a power system. This was mostly done using the database *IEEExplore*, but also *Researchgate* was used to discover additional papers. The conclusion of the project was that using LFAC seemed a viable solution for mid-range power transmission from OWFs. Some of the material from the specialization project report is partly reused for this thesis

ability to be read as an independent piece of work.

1.4 Structure

Chapter 2 describes the background for choosing *Horns Rev 3* as a case study for this thesis, and how it is designed. Chapter 3 describes the theoretical background for wind power and the issues regarding AC cable transmission. Chapter 4 describes the construction of the simulation model, and the parameters used. The results are presented and commented in chapter 5 using different cable lengths and variations in reactive power compensation. Chapter 6 discuss the overall results and suggests additional improvements for future development of LFAC offshore wind farms. The thesis then concludes and suggests further work in chapter 7.

In appendix A, complete tables of the different power flows are presented, in addition to enlarged figures of the voltages and currents in the cable at different lengths and frequencies. The four main types of wind turbine generators are presented in appendix B. Appendix C presents how the DQ-transformation for a three-phase system is developed.

Chapter 2

Horns Rev 3 Offshore Wind Farm

The case used to study the power system of an offshore wind farm is *Horns Rev 3* (*HR3*), located outside of Denmark, see map in figure 2.0.1, which is currently under construction and is to be in operation from 2019 [12][1]. The farm will consist of 49 turbines with a total capacity of 406.7 MW. The turbines that are to be installed is the Vestas *V164-8.0MW*.

The converters in the turbines can produce a nominal voltage of 33-35 or 66 kV directly from the converter. For *Horns Rev 3* the power is collected at 33 kV and then transformed to 220 kV before being sent through a subsea cable to the onshore connection.

The reason for choosing *HR3* as a basis for this thesis is the use of the Vestas *V164, 8.0 MW* turbines and the fact that *HR3* is designed for connection to shore using an AC export cable. The turbine recently set a world record for 24-hour power production of 216 MWh in December 2016 [13]. In this thesis, first the real length of the export cable of 35 km is used for simulations, and then the distance is increased to 100 km, 200 km and 300 km to check how a wind farm with the equivalent topology and parameters would function at a distance further off shore. This is used to investigate how the proposed low frequency technology would function on a real project being developed, but the thesis can also be read in more general terms to assess low frequency alternating current (LFAC) as a viable solution for power transmission through cables. All scenarios also include a 44.8 km onshore power cable connecting the substation to the transformer in Endrup, Denmark.

[1]The reference is dated June 2016, but confirmed on the Danish version of the websites, January 2017. English reference is chosen for readability purposes.

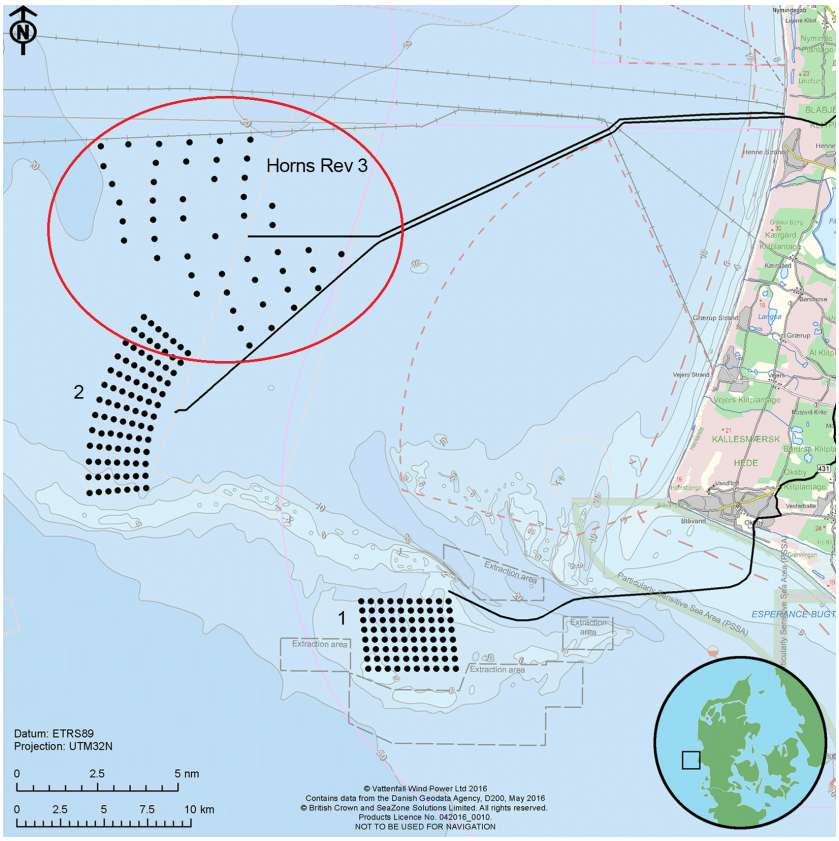

Figure 2.0.1: Map of Horns Rev 1-3. *HR3* in the upper left quadrant. Expanded view in the lower right corner showing Denmark and location of the wind farm [12]

2.1 Topology and Data of Horns Rev 3 OWF

The information on the topology of *HR3* is gathered mostly through *Horns Rev 3 - Technical Project description for the large-scale offshore wind farm (400 MW) at Horns Rev 3*, by *Energinet* [14]. Additional information has been provided by the Project Manager of *HR3* at *Energinet*, Søren Juul Larsen and Senior Grid Analyst, Christian Flytkjær Jensen.

49 turbines are distributed to the three offshore substation transformers, giving a distribution of 16, 16 and 17 turbines connected to each transformer. The voltage is stepped up from 33 kV to 220 kV at the offshore substation before being exported through a 35-km offshore cable. Onshore there is a static shunt reactor with a rating of 120 MVar connected, before the 44.8 km onshore cable connects to the onshore transformer stepping up the voltage from 220 kV to 400 kV. At this bus there are also connected two adjustable reactors, each with a rating of 60-120 MVar.

The single line diagram, without the 33 kV array, is shown in figure 2.1.1. Node 1-5 is used in calculating the power flow at the different nodes in the simulations.

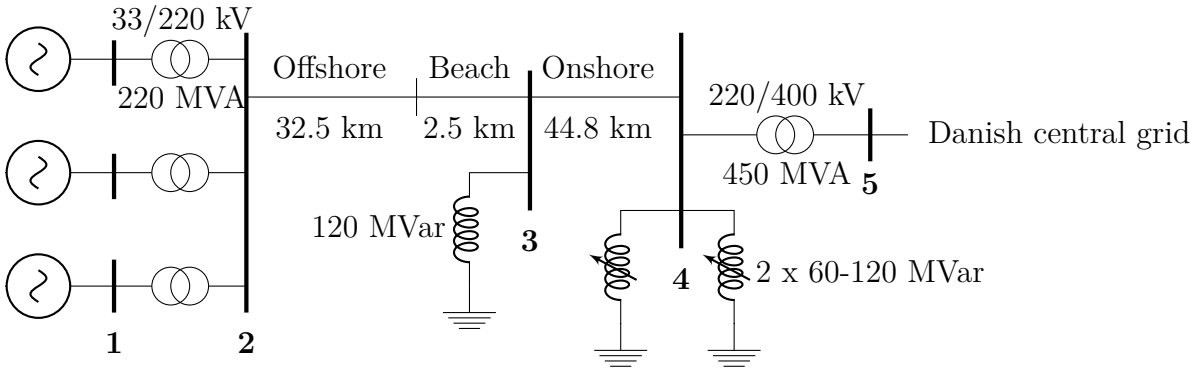

Figure 2.1.1: Aggregated single-line diagram of *HR3* [15]

2.1.1 Wind Turbines

The wind turbines to be used are the Vestas *V164, 8.0 MW*. The turbine data is listed in table 2.1.1 [12].

Table 2.1.1: Vestas *V164-8.0 MW* technical data [12]

Parameter	**Value**
Voltage	33 kV
Maximum capacity	8.3 MVA
Generator type	PM, Type 4 (see section 3.2.1)
Rotor blade length	80 m
Blade diameter	164 m
Maximum height	187.1 m
Cut-in wind speed	4 $\frac{m}{s}$
Nominal wind speed	approx. 14 $\frac{m}{s}$
Cut-out wind speed	25 $\frac{m}{s}$
Operational rotor speed	4.8 - 12.1 rpm
Auxilary power transformers	3 x 33/0.4 kV
Back-up diesel generators	✓

2.1.2 Offshore Substation Platform

The 33-kV array cables connecting the wind turbines to the substation is connected to the 220-kV export cable via three transformers, each with a rating of 220 MVA [14], as shown in the single line diagram in figure 2.1.1.

As can be seen by the single line diagram, there is no reactive power compensation located at the offshore substation.

The data for the offshore substation is given in table 2.1.2 [16].

Table 2.1.2: Offshore substation data [16]

Parameter	**Value**
Foundation type	Jacket
Foundation weight	1 500 t
Topside weight	1 800 t
Topside dimensions ($L \times W \times H$)	$36 \times 24 \times 17$ m
Number of transformers	3
Transformer power	220 MVA
Transformer ratio	33/220 kV
Switchgear	33 and 220 kV GIS
Auxilary power transformers	3 x 33/0.4 kV
Back-up diesel generators	✓

2.1.3 Cables

There are two types of submarine power cables used for the *HR3*, namely the 33 kV inter-array cables and the 220-kV export cable. The 44.8-km onshore cable has the same parameters as the offshore 220-kV cable.

2.1.3.1 Inter-Array Cables

For each row of 8-10 turbines there will be a medium voltage inter-array cable connecting the turbines to the transformer station [14]. The inter-array cables will be aluminum three core type with steel armor. The length and diameter will depend on the number

of turbines connected to it and the distance between them. The data for the inter-array cables are unknown. As mentioned describing the limitations of this thesis, the inter-array cables are excluded from the simulation model.

2.1.3.2 Export Cable

The export cable from the offshore substation discussed under section 2.1.2 to the onshore connection at *Blåbjerg substation* will use a three core 220 kV cable with a length of approximately 35 km. The cable will be a 3×2000 mm^2-Al conductor, with parameters given in table 2.1.3 [15].

Table 2.1.3: 220-kV cable data [15]

Parameter	**Symbol**	**Value**
Voltage	V	220 kV
Current	I	1 099 A
Resistance per length	R'	0.0392 Ω/km
Inductance per length	L'	0.350 mH/km
Capacitance per length	C'	219 nF/km

Figure 2.1.2: Offshore substation at *HR3* ©Energinet.dk

2.1.3.3 Onshore Cable

According to Christian Flytkjær Jensen, Senior Grid Analyst at *Energinet* [15], the export cable will be connected to a bus onshore where it will be extended 44.8 km through an onshore equivalent cable ending at the grid transformer, transforming the voltage from 220 kV to 400 kV.

2.1.3.4 Grid Transformer

The grid transformer has a rating of 450 MVA and transforms the voltage from 220 kV to 400 kV. The resistance of the windings in the transformer is $R_1 = R_2 = 0.007265$ pu and the inductance is $L_1 = L_2 = 0.0334$ pu [15]. The exact values of the equivalents in the magnetizing branch are unknown, but for the simulations, the magnetizing resistance is set to $R_C = 870$ pu and magnetizing inductance is set to $L_M = 50$ pu as this was used in a master thesis from 2015 done at the *Department of Electric Power Engineering* at the *Norwegian University of Science and Technology (NTNU)* [17]. In figure 2.1.3 the equivalent circuit of an ideal transformer is shown, where N_1 and N_2 are the number of turns of each of the two windings in the transformer.

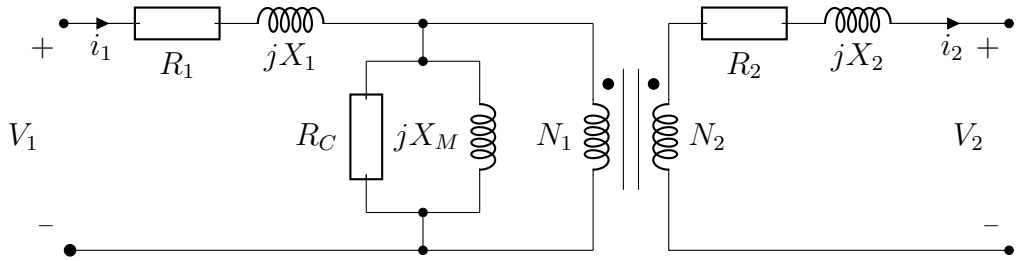

Figure 2.1.3: Ideal Transformer

2.2 Grid Code Requirements and Point of Connection

The Danish Transmission System Operator (TSO), *Energinet*, sets the grid codes for the power producers on the requirements for power quality throughout the lifetime of the wind farm. There are specific demands for wind power plants connected to the grid with ratings above 11 kW, as described in *TR 3.2.5 for wind power plants above 11 kW* [18].

The demands apply for the point of connection (POC), and for *HR3* the POC is defined as the 33 kV bussings on the low-voltage side of the offshore substation transformer.

In addition to the general requirements for wind power plants there is an agreement for *HR3* between the TSO, *Energinet*, and the power producer, *Vattenfall*, that there should be no reactive power delivered or consumed at the POC from *HR3*, meaning $Q_{\mathrm{POC}} \approx 0$ MVar.

Chapter 3

Wind-, Reactive Power Theory and Frequency Effects on Components in the Power System

This chapter introduces the theory of wind power extraction and the implications of using AC transmission systems. All details will not be covered in this chapter, but serve as insight in the various aspects that affect power extraction from wind and the transmission of power to the grid.

3.1 Aerodynamic Efficiency, Yaw Control and Pitch/Stall Regulated Turbines

The power that can be extracted from a wind turbine is given as

$$P = \frac{1}{2} \cdot \rho \cdot A \cdot C_p(\lambda, \beta) \cdot U^3 \tag{3.1.1}$$

Where P is the power in Watts, ρ is the air density (normally given at 1 atm, 15℃) in $\frac{kg}{m^3}$, A is the area swept by the blades in m^2, $C_p(\lambda, \beta)$ is the power coefficient as a function of the tip speed ratio, λ, and blade pitch angle, β, and U is the wind speed in $\frac{m}{s}$.

The maximum theoretical aerodynamic efficiency, known as the *Betz limit*, has the value

of $C_{p,max}(\lambda, \beta) = \frac{16}{27} \approx 0.5926$ [19].

The power output is highest when the wind direction is perpendicular to the turbine plane. A wind-vane on top of the nacelle senses the direction of the wind and the yaw control turns the turbine so that it achieves maximum power output. The yaw control can also be used to turn the turbine away from the wind if the power output is too high.

For wind speeds below rated speed, the optimal power output (optimization of C_p) is desired and the blades can adjust its pitch using motors in the turbine blades, changing the angle of attack between the wind and the blade, hence changing C_p. When reaching rated power output, the pitch control is used to lower the power coefficient, keeping the power output at its upper limits, for wind speeds above the rated wind speed. This is shown in figure 3.1.1, where the power output for the pitch-regulated turbine is kept constant, as indicated by the dashed line.

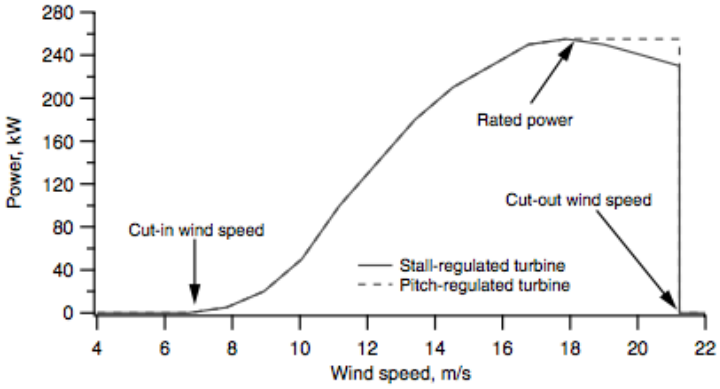

Figure 3.1.1: Pitch vs. stall regulated power output [19]

Stall-regulated turbines use a passive type of power control. The blades are designed such that when the wind speed increases above a certain value, the airfoil generates less aerodynamic force, eventually stalling, hence decreasing the power coefficient and power output [20].

For very high wind speeds the turbine need to be stopped to avoid damage. This is indicated in figure 3.1.1 where the cut-out wind speed for the illustrated turbine is 21 m/s. The turbines usually have a mechanical break that is used for stopping the rotation of the blades.

3.2 Wind Turbine Generator (WTG) Types

There are several different options regarding what types of generator arrangements that can be used in modern wind farms. There are two significant classes of turbines with regards to the speed control ability, it is the fixed speed and variable speed turbines [21]. In the early development of wind energy, the majority of wind turbines were operated at constant speed, while later development has preferred the use of variable speed operation.

Modern WTGs are divided into four distinct types depending on their topology and connection to the collection grid. There is also a fifth type using a variable speed drive train connected to a torque/speed converter coupled with a synchronous generator [20].

The only type presented in the thesis is type 4. For further reference, wind turbine generator types 1-3 are described in Appendix B, on page 79.

3.2.1 Type 4 Generator, Fully Rated Power Electronic Converter

Type 4 wind turbines with fully rated converter topology, offers a great deal of flexibility when choosing a generator, as it decouples the rotation of the generator from the electrical grid using the back-to-back converter, as shown in figure 3.2.1. This allows the turbine to operate at variable speed, thus achieving the optimal C_p. The ability to control both active and reactive power flow makes this type of topology able to use any type of generator.

The Type 4 WTG has been constructed with wound rotor synchronous generators, with control of the field current and a high number of generator pole-pairs, as permanent magnet synchronous generators or as squirrel cage induction generators [20]. Synchronous generators are becoming more popular and the multipole permanent magnet synchronous generators (PMSG) seems to become the most adapted generator for larger WTGs (3-8 MW) in the future, however there is a risk of this not to turn out as expected as the topology could be sensitive to increased prices of the rare earth metals used in the permanent magnets [22]. The Vestas *V164-8.0 MW* uses a Type 4 PMSG.

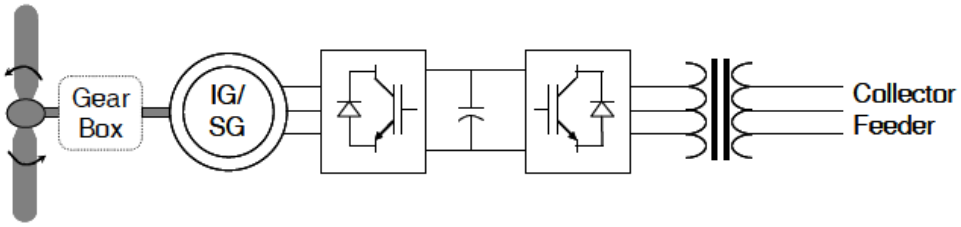

Figure 3.2.1: Type 4 WTG, Full converter [20]

3.3 Break-Even Distance

As will be discussed in section 3.4, the reactive power produced in AC cables presents a challenge with regards to maximum cable length.

However, converting the power to direct current (DC) presents large investments for constructing the converters. The choice of using an AC or DC transmission is a matter of costs. DC systems have smaller losses, but larger investment costs. This usually makes DC unsuited for short cable lengths where the benefits of low losses are lost in the increased investment costs.

At a given distance the costs for AC systems equals the cost of a DC system. This distance is known as the break-even distance. For cables, a typical break-even distance is approximately 100 km [23].

For illustration, one can regard the charging currents of the cable in a no-load situation without any reactive power compensation. Using the parameters for the $2000mm^2$ cable from table 2.1.3 and the no-load cable length given in equation (3.5.8), gives the result in equation (3.3.1).

$$l_{\text{max, no load}} = \frac{1\ 099\ \text{A}}{\frac{\sqrt{3}}{3} \cdot 220\ \text{kV} \cdot 2\pi \cdot 50\ \text{Hz} \cdot 0.219\mu\text{F/km}} \approx 126\ \text{km} \tag{3.3.1}$$

Equation (3.3.1) does not illustrate the actual break-even distance but it underlines the point that for long cables, the reactive current is substantial.

For distances shorter than the break-even distance, it is more cost effective to use AC transmission, while for distances longer than the break-even distance, it is cheaper to use DC transmission. A general example of the break-even/critical distance is shown in figure 3.3.1.

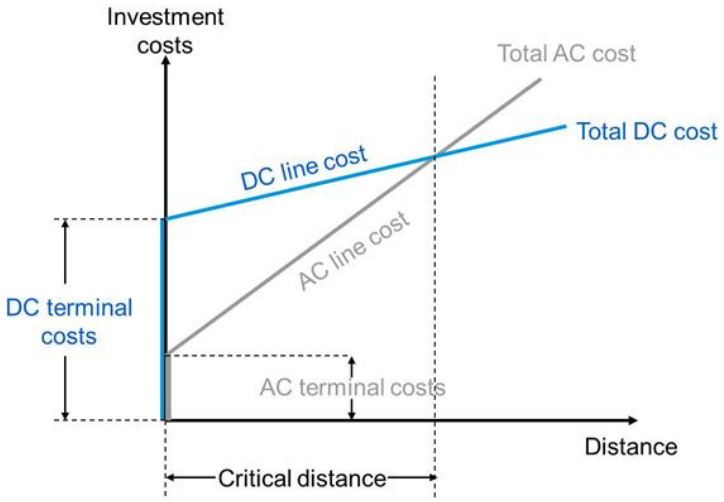

Figure 3.3.1: Illustration of break-even distance [24]

3.4 Alternating Current Systems

When the distance is less than 100 km from the offshore wind farm to the grid, high voltage AC (HVAC) three-phase transmission systems are generally used [23]. This is due to the low complexity and price of the components, and that the losses and reactive power compensation needed are acceptable. One can use standard three-phase cables, standard power electronics (PE) and transformers without the need for any additional offshore converter stations besides the PE found in the WTGs. If the distances get long, reactive power compensation is needed in one or both ends of the transmission cable. The easiest solution is to install reactive power compensation onshore, but in some scenarios there is need for compensation also at the offshore end of the cable.

3.4.1 Complex Power

For AC systems the concept of *apparent, active and reactive power* is introduced.

For a single phase circuit the complex/apparent power is given by

$$S = VI^* \tag{3.4.1}$$

$$S = P + jQ \tag{3.4.2}$$

$$|S| = |V||I| \tag{3.4.3}$$

Where V is the voltage given in Volt (V) and I is the current given in Ampere (A).

Apparent power is usually referred to as the magnitude of the complex power. P denotes the active power and is given in Watts. Active power is what we are able to utilize or consume in an AC-circuit. It is what most people refer to when they speak of the term electric power, in general.

One of the largest technical challenges regarding large-scale integration of offshore wind power in the existing power system, using alternating current transmission, is related to reactive power.

Reactive power for an AC-circuit, is for a sinusoidal current, equal to the product of the voltage and the current times the sine of the phase angle between these. Reactive power is not able to perform any work. It has the same dimension as that of active power and is measured in the unit Volt-Ampere-Reactive (Var).

The overall consideration/requirements regarding power production from offshore wind and the use of AC transmission, are related to voltage control and the control of reactive power.

This includes:

- Control of reactive power
- Control of voltage
- Flicker control
- 'Fault ride through' capability of the wind power plants

The amount of active power transferred through a transmission system is given by the voltage of the sending- and receiving end, V_S, V_R, the voltage angle between them, $\delta_S - \delta_R$ and the line impedance, X_{SR}.

$$P = \frac{V_S V_R}{X_{SR}} \sin(\delta_S - \delta_R) \tag{3.4.4}$$

3.4.2 Magnetic Fields

Different materials have different properties regarding how easily they are magnetized. Materials with high magnetic conductivity are beneficial to use in electrical equipment where there is need for large magnetic fields, such for instance in the core of a power transformer. This property is denoted by the magnetic permeability μ of a material, $\mu = \mu_r \cdot \mu_0$, where μ_0 is the magnetic permeability of vacuum and μ_r is the relative permeability of the material.

$$\mu_0 = 4\pi \cdot 10^{-7} \text{ Ns}^2/\text{C}^2$$

For ferromagnetic materials, the relative permeability is large, ranging from approximately $\mu_r = 10^5$ for iron, to $\mu_r = \infty$ for ideal magnetic conductors. The relationship between magnetic flux density and permeability is given by $\mathbf{B} = \mu\mathbf{H}$, where $\mathbf{H}$ is the magnetic field given in Ampere/meter.

For a coil, the amount of magnetic flux, Φ_B, is related to the current passing through the conductor, I, and the number of turns, N.

$$\Phi_B = N \cdot I = \mathbf{B} \cdot A = \mu \cdot \mathbf{H} \cdot A \tag{3.4.5}$$

$$\mathbf{H} = \frac{N \cdot I}{\mu \cdot A} \tag{3.4.6}$$

3.4.2.1 Magnetic Induction

The total magnetic flux of an area is denoted by $\Phi_B = \mathbf{B} \cdot A$, and is measured in Weber (Wb), where A equals the area and B is the magnetic flux density, measured in Tesla (T).

Faradays law of induction (equation (3.4.7)), gives the basis for all transformer (and generator) operation. The law states that the induced electromotive force in any closed

circuit is equal to the rate of change of the magnetic flux enclosed by the circuit. As the rate of change of the magnetic flux is affected by the frequency of the current, the operating frequency would affect the induced voltage, given constant current of the coil and the area of the core. For a tightly wound coil of wire composed of N identical turns, with the same magnetic flux, the resulting electromagnetic force (EMF) equals

$$e(t) = -N \cdot \frac{d\Phi_B}{dt} \tag{3.4.7}$$

where $e(t)$ is the EMF given in volts at any given instant of time, and Φ_B is the magnetic flux of a single turn of the enclosing coil wire.

3.4.2.2 Hysteresis

The amount of magnetic polarization in a material is indicated by $\mathbf{M}$. For materials that are not permanent magnets this magnetization is related to the application of a magnetic field $\mathbf{H}$. The first time the material is magnetized, it goes from a magnetization of zero to a value given by the applied magnetic field. For ferromagnetic materials, the permeability is not linear, and after applying a certain magnetic field the material gets *saturated*. The permeability decreases and despite adding a stronger magnetic field, the amount of magnetization does not increase proportionally. When decreasing the magnetic field, the magnetization goes down, but it does not follow the same path as when magnetized. When there is no applied magnetic field, there is still magnetization of the material. This is called the remanent magnetism of the material, and is the reason why after applying a magnetic field from for instance a permanent magnet to a piece of iron, the iron will act as a magnet, even after removing the permanent magnet. When applying an opposite magnetic field the magnetization changes direction, but the material will now have a remanent magnetic field the opposite way after removing the magnetic field. The magnetic remanence gives basis for the hysteresis curve illustrated in figure 3.4.1.

3.4.2.3 Magnetic Energy and Losses

The magnetic energy of a infinitesimal volume is given by $w_m = \frac{1}{2} \cdot \mathbf{B} \cdot \mathbf{H}$ which gives that due to hysteresis, there is a power loss for each cycle equal to the area of the hysteresis

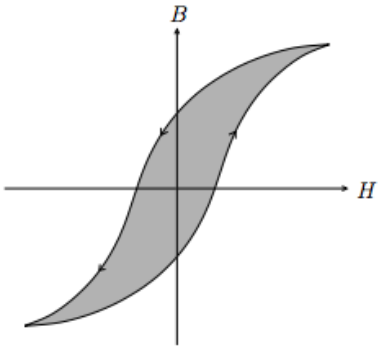

Figure 3.4.1: Hysteresis curve

curve times the volume of the flux path (usually the transformer core). Hence the power losses due to hysteresis is proportional to the operating frequency, f.

3.5 AC Cables

Modern three-phase HVAC cables are usually cross-linked polyethylene cables (XLPE). The cables are reinforced with an armor if the cables are to be used in subsea applications. This is important to be able to withstand the mechanical tension from its own weight when laid from vessels, at depths of up to several hundred meters, and to protect the cable from impacts from for instance trawls, anchors etc. The cables are usually buried in trenches in the seabed, to provide extra protection.

3.5.1 Reactive Power Production and Consumption in AC Cables

Figure 3.5.1 depicts a π-equivalent circuit, which is a per phase representation of medium length transmission cables. The current carrying capacity of the cable is given by its thermal limits, and if the power factor of the system, the relationship between active and apparent power is different from unity, there is also a reactive component of the current. The magnitude of the total current is given by:

$$I_{Total} = \sqrt{(I_P)^2 + (I_Q)^2} \tag{3.5.1}$$

Where I_P is the active and I_Q is the reactive component of the current in the circuit.

Assuming a lossless cable ($R = 0\ \Omega$), with a per phase representation as shown in figure 3.5.1, the reactive power in the cable can be described by the following relationships:

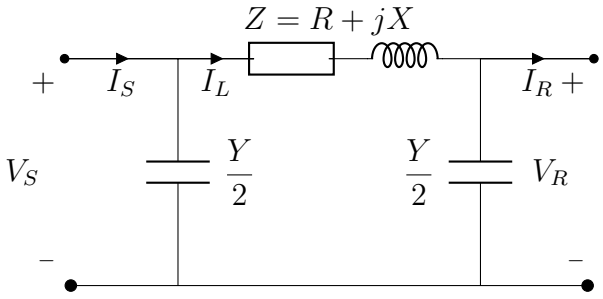

Figure 3.5.1: π-equivalent

$$Q_{ph,produced} = (\frac{V_S}{\sqrt{3}})^2 \cdot B = \frac{V_S^2}{3} \cdot \omega \cdot C' \cdot l \Rightarrow Q_{prod} = 3 \cdot Q_{ph,prod} = V_S^2 \cdot \omega \cdot C' \cdot l \quad (3.5.2)$$

$$Q_{ph,consumed} = I^2 \cdot X_L = I^2 \cdot \omega \cdot L' \cdot l \Rightarrow Q_{consumed} = 3 \cdot I^2 \cdot \omega \cdot L' \cdot l \quad (3.5.3)$$

$$Q_{consumed} = Q_{produced} \quad (3.5.4)$$

$$V_S^2 \cdot C = I^2 \cdot L \Rightarrow I = V_S \cdot \sqrt{\frac{C'}{L'}} \quad (3.5.5)$$

$$P_{SIL} = V_S^2 \cdot \sqrt{\frac{C'}{L'}} \quad (3.5.6)$$

Where $\omega = 2\pi \cdot f$ and f is the frequency given in Hertz, C' is the per length capacitance given in $\frac{F}{km}$, l is the cable length in km, V_S is the line to line voltage and L' is the per length inductance given in $\frac{H}{km}$. P_{SIL} is the surge impedance loading of the cable, the active power transferred when the reactive power production in the cable equals its consumption.

For an open-end cable, assuming a flat voltage profile, the capacitance per length value and the length of the cable is the only parameter of importance. A flat voltage profile implies that $V_S = V_R$ and hence there is no current passing through the resistor and inductor. The reactive power produced at no-load, with a line to line voltage V_S, is then given by equation (3.5.7).

$$Q_{ph,\text{ no load}} = \frac{V_S^2}{3} \cdot \omega \cdot C \cdot l \Rightarrow I_{ph,\text{ no load}} = \frac{Q_{ph}}{\frac{V_S}{\sqrt{3}}} = \frac{\sqrt{3}}{3} \cdot V_S \cdot \omega \cdot C \cdot l \quad (3.5.7)$$

This implies that a large amount of the current carrying capacity of the cable is used for transporting reactive power. At no-load, this current is directly proportional to the frequency of the cable. When only considering the reactive power produced, and its implications on the limitations in cable lengths, it seems that it is beneficial to use as low voltage as possible. However, this increases the current in the cable and the capacity to transfer active power drops significantly as there will be a higher power loss in the cable. For long distance cable transmission, the current is therefore transmitted at as low frequency as possible, with a frequency of zero the current is then a direct current (DC).

For a cable with a given current rating, capacitance per length, voltage rating and frequency, the maximum cable length at no-load is given by equation (3.5.8), which was

used to calculate the no load length of the 220-kV cable in equation (3.3.1).

$$l_{\text{max, no load}} = \frac{I}{\frac{\sqrt{3}}{3} \cdot V_S \cdot 2\pi \cdot f \cdot C} \tag{3.5.8}$$

For longer cables (typically longer than 100 km) the parameters need to be adjusted as the π-model shown in figure 3.5.1 is not accurate enough. The long-line model (also known as distributed parameter model) is developed using differential equations describing the line. The modified π-model, looks the same as the π-model, but uses the modified parameters Z' and Y' instead of the ordinary parameters. The relationships between them are given in equation (3.5.9) and (3.5.10).

$$Z' = Z \cdot \frac{\sinh \gamma l}{\gamma l} \tag{3.5.9}$$

$$Y' = Y \cdot \frac{\tanh(\gamma \cdot l/2)}{\gamma \cdot l/2} \tag{3.5.10}$$

where $\gamma = \sqrt{y \cdot z}$ is the propagation constant of the line, given as the square root of the product of the shunt admittance, y, and series impedance, z, per km line.

3.5.2 Reactive Power Compensation

The reactive power compensation units are used for improving the power transmission efficiency, reliability and security of the system [25]. If having an offshore platform or hub with enough available space, the reactive power compensation is usually placed here in addition to the compensation onshore supplying reactive power to the cable from both sides. The leading device for shunt connected compensation is the static compensator (STATCOM) [26].

3.6 Different Possible LFAC Topologies for Offshore Wind

With regards to offshore wind farms there are two main concepts for topologies that can be chosen for the LFAC transmission system. These concepts can be described as either a full LFAC system, from generator to the back-to-back converter onshore, or as an ordinary system with a frequency converter in both ends of the export cable, both offshore and onshore, converting the frequency to 16.7 Hz for the transmission cable only.

The first option implies that the wind turbines and generators will have to adjust the PE-converter in each WTG so that it delivers power at the desired frequency. The offshore collection grid, the transformers and power cable will operate at a lower frequency and the individual WTG would preferably employ Type 4 synchronous generators with fully rated converters [23].

The second option implies that for all purposes, the only exception from a 50 Hz system, is the frequency converter offshore and onshore, and the LF operation of the transmission cable. This topology resembles the HVDC topology as there is need for a converter station offshore, but it opens for the benefits of breaking an alternating current instead of a direct current.

The full LFAC topology is the only one that will be further investigated in this thesis. According to the specialization project report from the *Norwegian University of Science and Technology, NTNU* [11], conducted in 2015 by the author of this thesis, it was concluded that the full LFAC topology was the most viable option for the use of LFAC offshore.

3.7 LFAC Effects on Power System Components

In a paper published in 2015, *Erlich et. al* [23] propose an alternative to the existing 50/60 Hz AC and HVDC technology. It is proposed that a lower frequency of 16.7 Hz can be used for the collection grid, the main transformer, and the export cable linking the offshore network with the onshore grid, as depicted in figure 3.7.1. The main onshore converter would be implemented as a back-to-back converter. The frequency of 16.7 Hz is

chosen due to its use in the railway system in Scandinavia and other parts of Europe, so there already exists components that can be investigated and compared with the normal operating frequency of 50 Hz. Although the components are often single-phase and proper investigations and qualification will be needed before commercialization is possible. This frequency is also located somewhere between 0-Hz (DC) and normal AC operating at 50- or 60 Hz.

In this section, the different components and their behavior with regards to operating at a lower frequency are described.

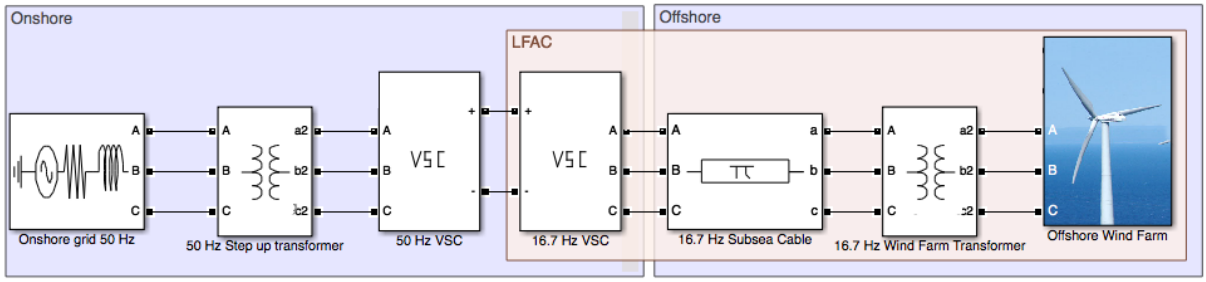

Figure 3.7.1: Full LFAC topology (illustration made using MATLAB/Simulink [27])

3.7.1 Generator

Wind turbine generators can generate AC at a frequency of 16.7 Hz if it is connected to the collection grid through a fully rated PE converter, such as for Type 4 WTGs [28]. The frequency of the generator is decoupled from the frequency in the collection grid using a fully rated PE converter, and hence a lower operational frequency of the collection grid does not affect the generator in this case.

3.7.2 Power Electronic (PE) Converters

The PE-converters are not much affected by the operating frequency.

When reducing the frequency in the grid, the switching frequency of the converters can also be lowered, reducing the switching losses. If the switching frequency is kept constant, reducing the output frequency in the grid would give a better modulation of the voltage and less harmonic components in the system. The choice of switching frequency will

essentially be a tradeoff between the power switching losses in the converter and harmonic distortion in the grid.

3.7.3 Cables

One of the main reasons for choosing LFAC compared to normal frequency AC, is due to the reactive power production of the cable and the fact that substantial amounts of the current carrying capacity of the cable is used for transmitting reactive power. The main limiting factor when considering long-distance HVAC cable transmission is the charging of the cable due to the reactive power [29]. The effect of reactive power production in cables have already been described in section 3.5.1, by equations (3.5.1) to (3.5.8). In LFAC systems the reactive power in the cable will be considerably lower.

For LFAC systems the cables used for normal AC applications can be used without alterations [30]. The losses in the cable will by reducing the frequency to 1/3 of the normal 50 Hz frequency be reduced due to a reduction of losses in the sheath, dielectric losses and better utilization of the entire cross section of the conductors due to reduced skin effect [31]. Also, the thermal ratings will be better under the same environmental conditions.

The dependency of frequency is given in relation to the charging currents at high frequencies and problems with regards to charge accumulation is only to be considered for very low frequencies (below 0.1 Hz) [32] and will not be discussed further in this report. For frequencies above 1 Hz the effect of surface charge accumulation is negligible [33], and is of that reason for all purposes neglected in this thesis.

In 2010 manufacturers offered to provide cables of up to 400 kV [34], cables that without modifications, can be used for the LFAC application described. In 2014 AC cables of up to 550 kV are also available [35], but there has not been found any available technical parameters for such cables to assess how the cable operates and the cable limitations.

3.7.4 Transformers

Before discussing the impact of a frequency change in the operation of a transformer there is need to understand one of the fundamental laws describing transformer operation.

The total magnetic flux of an area is denoted by $\Phi_B = \mathbf{B}A$ and is measured in Weber (Wb) where A equals the area in m^2 and B is the magnetic flux density, given in Tesla (T).

Faradays Law of induction, equation (3.4.7)/(3.7.1), gives the basis for all transformer operation. The law states that the induced electromotive force (EMF) in any closed circuit is equal to the rate of change of the magnetic flux enclosed by the circuit. For a tightly wound coil of wire, composed of N identical turns with the same magnetic flux, the resulting EMF equals

$$e(t) = -N \cdot \frac{d\Phi_B}{dt} \tag{3.7.1}$$

$$E_{\,\mathrm{RMS}} = 4.44 \cdot f \cdot N \cdot \Phi_{B,peak} \tag{3.7.2}$$

where $e(t)$ is the EMF at any given time in volts, and Φ_B is the magnetic flux of a single turn of the enclosing coil wire. $E_{\,\mathrm{RMS}}$ is the *Root Mean Square* voltage of a sinusoidal flux, varying at a frequency f.

For the transformers to be able to transform the same amount of power at a lower frequency, the total rate of change of magnetic flux need to be held constant, as described by equation (3.7.1). Either the area of the transformer core or the number of windings need to be increased, or the magnetic flux density properties of the steel used in the transformer core need to be enhanced, to avoid magnetic saturation. This makes the transformer heavier and costlier as it requires either more copper for the windings or more (or better) steel in the transformer, increasing its size.

For an operating frequency of 16.7 Hz the number of turns must be tripled, the area of the core must be tripled or the steel of the transformer core must have better magnetic properties. However, a preliminary concept study by *Erlich et al.* [23] shows that 16.7 Hz transformers are only twice heavier than comparable 50 Hz transformers, which is also indicated by *Wyllie et al.* [36].

Wind farm substation transformers for LFAC operation was designed by *Wyllie et al.* in [36] based on a 250 MVA 50 Hz design, transforming 132/33 kV. There were two options discussed, either a wide or tall transformer design. Varying the number of turns, rather than changing the core diameter, gave a significantly lighter design for the LFAC transformer. The tall design, increasing the number of turns weighed 253.9 tons, as

compared to the wide design increasing the core diameter weighing 413.8 tons. The reference 50 Hz transformer weighed 143.4 tons, giving an increase in weight from 50 to 16.7 Hz of 77 % for the tall design. Figure 3.7.2 depicts the wide and tall design.

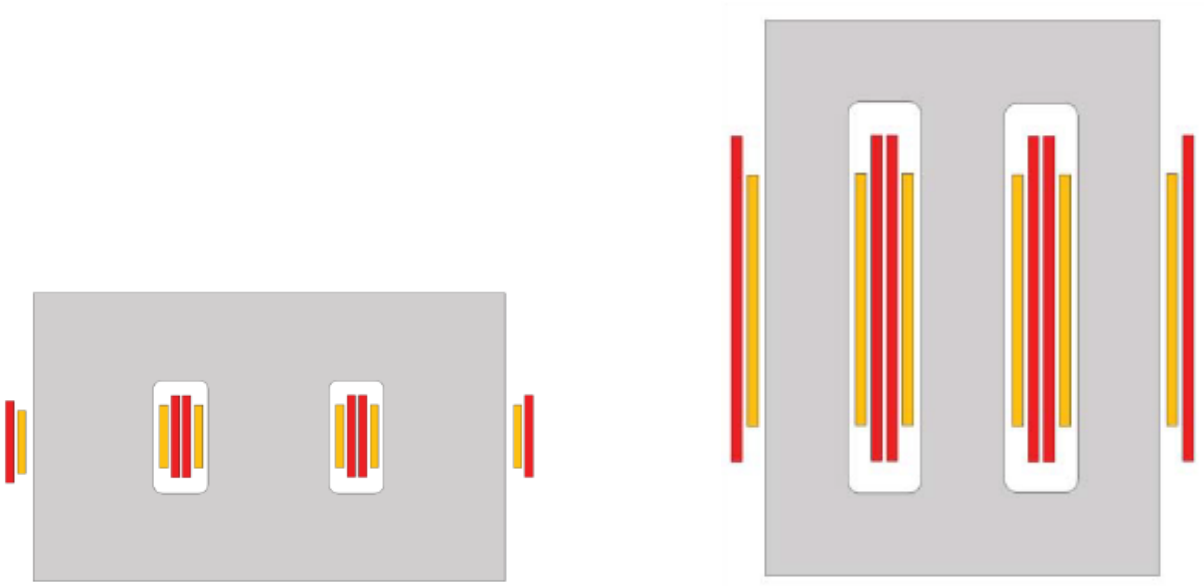

(a) Wide design, LFAC 16.7 Hz transformer

(b) Tall design, LFAC 16.7 Hz transformer

Figure 3.7.2: Different LFAC 16.7 Hz transformer designs [36] (Not to scale).

For the full LFAC topology shown in figure 3.7.1, also the individual transformer in each turbine, if using another type of wind turbine than Type 4, must operate at 16.7 Hz [36]. Due to space limitations in the WTG the transformer would most likely not be placed inside the nacelle, but in the tower. A tall design would increase the weight of about 108 %, but the volume would also increase by approximately 107 % [36]. This will probably make the transformer too large and heavy to be placed in the nacelle, but it can instead be placed in the tower [23]. The placement of the transformer varies from the different producers.

For inductive and capacitive components used for compensation, the reduction in reactive power consumed or produced is proportional to the frequency. According to *Erlich et. al* [23], the most significant problem for LFAC transmission systems seems to be the increased size and weight of the transformers and reactors.

3.7.5 Breakers and Switchgear

The operation of breakers and switchgear has according to *Canelhas et. al* [37] not been considered to be a problem in LFAC applications. Regarding re-striking due to large recovery voltages across the breakers, the use of lower frequency would reduce the risk of re-strikes after opening the breaker due to the voltage not rising as fast as for normal AC operation, giving the connectors in the breaker longer time to separate.

Chapter 4

Simulation Model and Parameters

This chapter describes the construction of the simulation model, and lists the parameters used for the different simulations.

The simulations are done using *MATLAB* [27] equipped with *Simulink* and the *Simscape/Powersystems* package. The topology used for the simulations is depicted in figure 4.0.1, where blue indicates 33 kV, green indicates 220 kV and yellow indicates 400 kV.

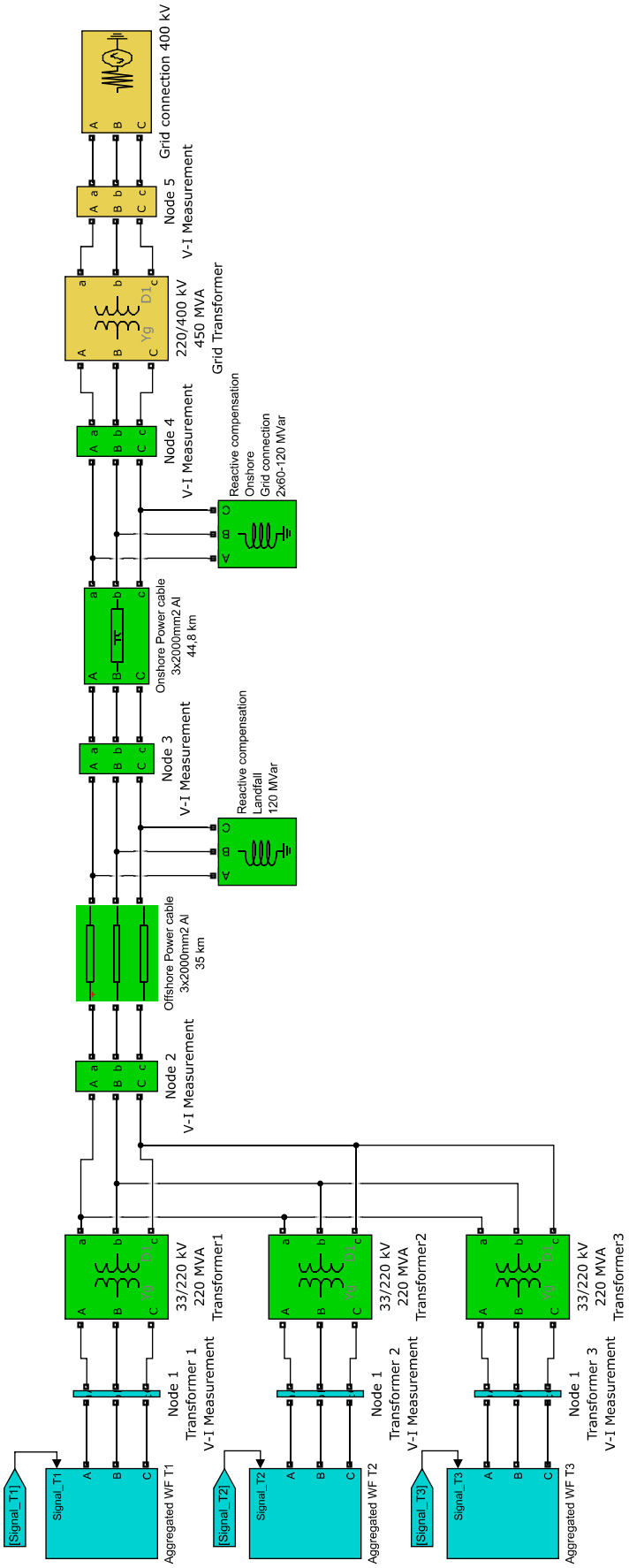

Figure 4.0.1: Simulation Topology for *Horns Rev 3*

4.1 Model Limitations

The model does not include the converters in the WTG. The aggregation of several WTGs is modelled as three current controlled voltage sources.

For the actual LFAC operation ($f = 16.7$ Hz) there would be a back-to-back converter before the grid connection to convert the frequency back to 50 (or 60) Hz. This is not included in the simulations and hence the simulation is done with all the components in figure 4.0.1 operating at the same frequency.

The grid code requirements, mentioned in section 2.2 on page 12, gives the reactive power delivered/consumed by the wind farm to be $Q = 0$ MVar. In the simulation model this can either be achieved by changing the setpoints for the currents of the dq-axes, or by reactive compensation. Particularly the setpoint for the q-axis current is important for the reactive power from the WTGs. As there has been no success discovering what ensures the grid requirements with regards to minimizing the reactive power flow, this is in the model simply done by keeping $i_q = 0$, before the POC at the 33 kV bussings at the low-voltage side of the substation transformers.

4.2 Model Structure

The model is constructed with the WTG's as current-controlled voltage sources based on measured output currents from the WTGs and base quantities derived from the desired power output.

The voltage sources are connected to a RL-filter.

The model uses standard components from the *Simscape/Powersystems* library, including:

- Controlled voltage sources
- Three-Phase Series RLC-branch (used as RL-filter)
- Three-Phase VI Measurement
- Three-Phase Transformer (two windings)
- Distributed Parameters Line

- Three-Phase Parallell RLC Load (used as shunt reactor)
- Three-Phase Voltage Source
- abc to dq0 Transformation
- dq0 to abc Transformation

In addition, the model uses a non-standard Phase-Locked Loop (PLL) for giving the angular position of the voltage vector of the onshore grid for synchronization of the voltage generated at the wind farm. The reason for using a non-standard component is that the standard component not being able to function properly on frequencies below approximately 30 Hz. The details of this component is not important and will not be described further, but the function is the same as the standard PLL. The PLL used in the simulations was developed by Santiago Sanchez for use in his PhD. - thesis [38].

Figure 4.0.1 depicts the nodes where the power flow is measured, but in addition the offshore power cable is split into four sections of equal length to monitor the voltage and current in the cable as the sending end and receiving end of the cable are not necessarily the most critical points.

4.2.1 Base Values

The base values in table 4.2.1 are calculated using rated apparent power and voltage of the WTG's given in table 2.1.1 in section 2.1.1 on page 9. The frequency affects the base value of the impedance L.

Table 4.2.1: Base values

Parameter	**Value** (50 Hz)	**Value** (16.7 Hz)
$V_{1,\text{ Base}}$	33 kV	33 kV
$S_{1,\text{ Base}}$	8.3 MVA	8.3 MVA
ω_{Base}	314.15 $\frac{rad}{s}$	104.72 $\frac{rad}{s}$
$I_{1,\text{ Base}}$	167.68 A	167.68 A
Z_{Base}	196.81 Ω	196.81 Ω
L_{Base}	0.6265 H	1.8794 H

The base value for the currents are then multiplied by the number of turbines connected to each transformer, and is used as current reference for the aggregated current-controlled

voltage sources.

4.2.2 Parameter Values

The parameters used for simulating the different frequency scenarios are given in table 4.2.2. The amount of reactive power compensation for the different cable lengths will be introduced in chapter 5, results.

The setpoint for the current from each of the three aggregated wind turbine clusters are based on the rated power of the number of turbines in each cluster, where two transformers are connected to 16 turbines while the last transformer is connected to 17 turbines, as described in detail in section 2.1 on page 8.

Table 4.2.2: Parameter values used for simulation

	Parameter	Description	Unit	Value (50 Hz)	Value (16.7 Hz)
Control and general	K_p	Proportional gain	pu.	1.5915	4.7746
	K_i	Integral gain	pu.	33.33	33.33
	L_{eq}	Filter inductance	pu.	0.15	0.15
	R_{eq}	Filter resistance	pu.	0.01	0.01
	L_{filt}	Filter inductance	H	0.0940	0.2819
	R_{filt}	Filter resistance	Ω	1.9681	1.9681
	f_{sw}	Converter switching frequency	kHz	10	10
	T_a	Analog response time	s	$1.5 \cdot 10^{-4}$	$1.5 \cdot 10^{-4}$
	τ	Time constant	s	0.0477	0.1432
Cable	L'	Inductance per length	mH/km	0.354	0.354
	C'	Capacitance per length	nF/km	227	227
Offshore Tr.	S	Rated apparent power	MVA	220	220
	R_{core}	Winding resistance	pu.	0.00265	0.00265
	$L_{leakage}$	Leakage inductance	pu.	0.0375	0.0375
	R_{mag}	Magnetizing resistance	pu.	870	870
	L_{mag}	Magnetizing inductance	pu.	50	50
Grid Tr.	S	Rated apparent power	MVA	450	450
	R_{core}	Winding resistance	pu.	0.007265	0.007265
	$L_{leakage}$	Leakage inductance	pu.	0.0334	0.0334
	R_{mag}	Magnetizing resistance	pu.	870	870
	L_{mag}	Magnetizing inductance	pu.	50	50

4.2.2.1 System of Differential Equations in the dq-reference Frame for a Two-Level Converter

Having a voltage source with an RL-filter gives the following relationship between the voltages, currents and cross coupling between the d- and q- axis. Figure 4.2.1 shows the equivalent circuit for the d-axis. Since the axes are orthogonal, the voltage over the inductor can be written as a function of the current in the other axis, and gives the basis for the difference in the term being added or subtracted. Equation (4.2.1) and (4.2.2) is reflected in the control system depicted in figure 4.2.2.

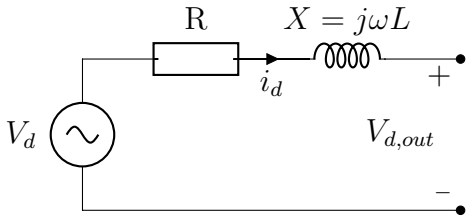

Figure 4.2.1: d-axis equivalent circuit

$$L \cdot \frac{di_d}{dt} = V_d - V_{d,out} - R \cdot i_d + \omega \cdot L \cdot i_q \tag{4.2.1}$$

$$L \cdot \frac{di_q}{dt} = V_q - V_{q,out} - R \cdot i_q - \omega \cdot L \cdot i_d \tag{4.2.2}$$

4.2.3 Control System

The control structure is depicted in figure 4.2.2 where the explanation on the d- and q-axis values can be read in appendix C on page 83. The reference for the d- and q-axis currents on each cluster is set as a per unit value, while the voltage reference giving the signal to the voltage sources are calculated using the control structure shown in figure 4.2.2.

The parameters for the proportional-integral controller (PI) listed in table 4.2.2 are calculated based on the *Modulus Optimum* criterion, which will not be described in detail. However, the parameters are based on the equations (4.2.3) to (4.2.5). Where R_{eq} is the filter resistance in Ω, L_{eq} is the filter inductance in H, ω_{Base} is the electrical angular velocity. τ is the time constant of the system, K_p and K_i are the proportional- and integral gain of the PI controller.

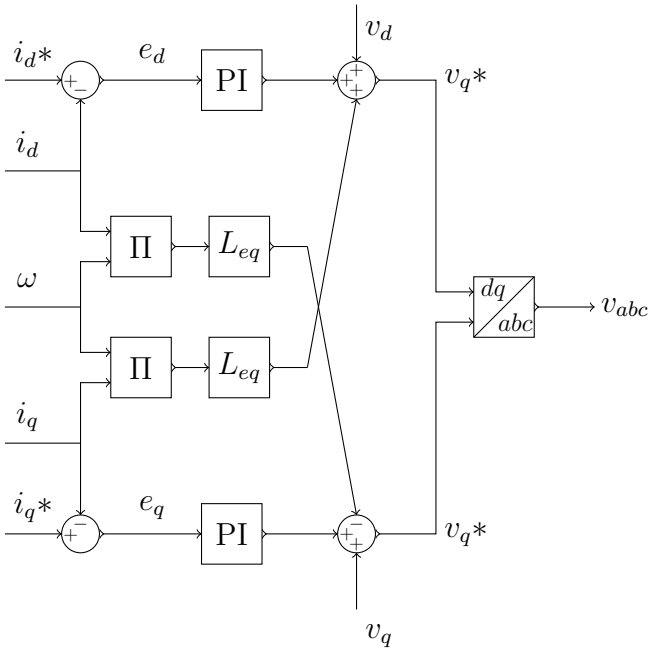

Figure 4.2.2: Current control and voltage references (in pu).

$$\tau = \frac{L_{eq}}{\omega_{Base} \cdot R_{eq}} \tag{4.2.3}$$

$$K_p = \frac{L_{eq}}{2 \cdot \omega_{Base} \cdot T_a} \tag{4.2.4}$$

$$K_i = \frac{K_p}{\tau} \tag{4.2.5}$$

Chapter 5

Results

In this chapter, the simulation results for different scenarios with respect to offshore cable length and reactive power compensation are presented. At the end of the chapter, in section 5.6 and 5.7, the results from *ABB* are presented regarding size and weight of the transformer and reactors operating with reduced frequencies.

The results are presented when the system has reached steady state, which occurs after about 1.2 seconds from starting the simulation. This can be seen in figure 5.0.1 that shows the dq-axis components of the control system and the power flow at node 5 for 50 Hz operation at $P_{1,\,\mathrm{ref}} = 1.0$ pu as shown in row 2 of table 5.2.1. The d-axis reference has a gradual increase in order to reduce oscillations, but since it is only steady-state that is investigated this does not affect the end results.

The most important results are presented in this chapter, and the complete tables showing the power flow for 80 %, 60 %, 40 % etcetera of the maximal power production at the wind farm at different offshore cable lengths, LFAC and normal AC, are placed in Appendix A on page 67. Section A.2 and A.3 in the appendix include enlarged figures showing the current in the cable at different points of the cable and voltage at the sending end, node 2.

The voltage limits for steady state operation is set to the equivalent of 1.1 pu. According to the standard *62062, Power cables with extruded insulation and their accessories for rated voltages above 150 kV up to 500 kV* by the *International Electrotechnical Commission (IEC)*, a cable with rated voltage 220 kV will be able to operate permanently at up to 245 kV or 1.114 pu [39]. The offshore cable in the simulation model is split into

four equal sections, measuring the voltage and current between each section to ensure operation within the rated limits of the cable.

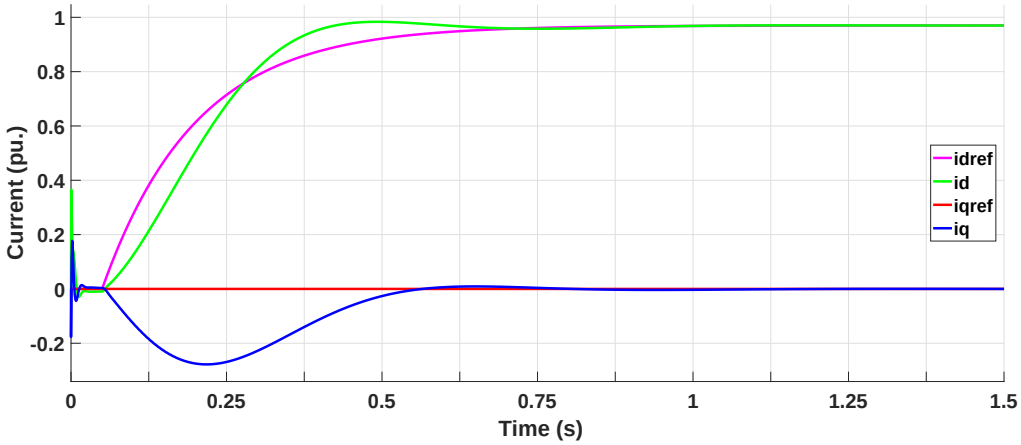

(a) dq-axes currents, reference and actual value

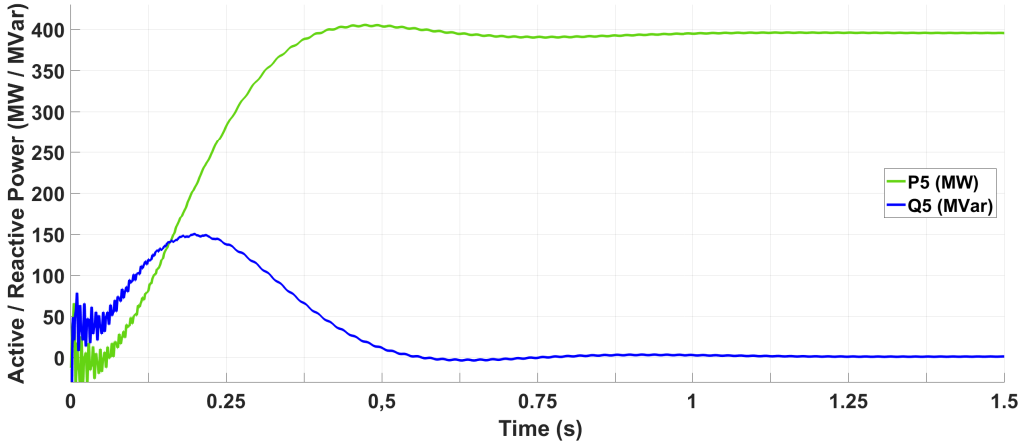

(b) P_5, Q_5

Figure 5.0.1: $P_{1,\,\mathrm{ref}} = 1.0$ pu, $Q_{3,\mathrm{comp}} = 120$ MVar, $Q_{4,\mathrm{comp}} = 97$ MVar, $f = 50$ Hz, $l_{\mathrm{offshore}} = 35$ km

5.1 Simulation of Different Scenarios

Following are the simulations from the different scenarios, varying lengths, reactive power compensation etc. In section 5.2, where the real cable length of 35 km is used, the reactive compensation in node 3 is static and set to 120 MVar for $f = 50$ Hz and 40 MVar for $f = 16.7$ Hz. The compensation in node 4 is then adjusted to stay within the limits of the variable reactors, which can operate between 60-240 MVar, and under the maximal

current rating of the cable, staying as close as possible to unity power factor at the grid connection in node 5.

For longer cable lengths, the reactive power compensation at node 3 and node 4 is adjusted so that the current in the cable stays within its rating of $I_{\text{RMS}} = 1\ 099$ A, as listed in table 2.1.3, section 2.1.3.2 on page 11. Previous limitations in the reactive compensation are disregarded for cable lengths longer than 35 km, and the reactor in node 3 is treated as a variable shunt reactor. The reactive compensation does not have to operate within certain limits, and this is to highlight the compensation needed for such cables to be able to operate. The aim of adjusting the reactive power compensation in the simulations is to achieve unity power factor at the connection to grid. In a realistic case, the reactive power compensators would be rated higher than the actual demand for compensation to open for the ability to consume reactive power from the central grid. The Danish grid codes state that for power production units above 1.5 MW, it is required to be able to operate with a power factor between 0.975 lagging and 0.975 leading [40].

The reference for the power generated at the offshore wind farm is based on currents in both the d- and the q-axis. Lowering i_d simulates reduced power production at lower winds, outages of parts of the wind farm or other scenarios where the wind farm operates below maximum capacity. Keeping $i_q = 0$ throughout the simulation ensures that the wind farm aims to keep $Q_1 = 0$ MVar. For all results showing operation below maximum power production capacity, please refer to Appendix A on page 67.

5.2 Horns Rev 3, Real Case

The actual topology of *Horns Rev 3* is depicted in figure 5.2.1.

In the real case, the offshore cable is 32.5+2.5 km long. The reactive power compensation at landfall, node 3, is a static 120 MVar shunt reactor. After that there is a 44.8 km onshore cable connected to two variable shunt reactors, that combined can operate between 60-240 MVar.

The current in the 35-km cable, with reactive power compensation at rated power, is depicted in figure 5.2.3.

The topology has been given numbers on the different nodes, starting with node 1 at the low voltage side (LV) of the offshore substation transformer. Node 2 is on the HV side

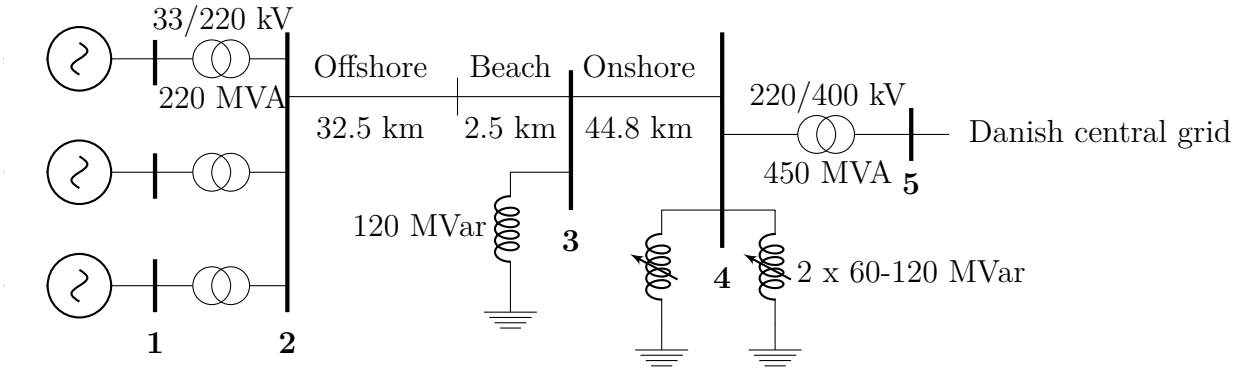

Figure 5.2.1: Aggregated single line diagram of *HR3* [15]

of the offshore transformers. Node 3 is located at landfall, the point of the 120 MVar reactive power compensation. Node 4 is on the LV side of the grid transformer, and node 5 is on the HV side. The rating of the grid transformer is 450 MVA.

5.2.1 Reference Case. Normal Length, 35 km, 50 Hz

Setting the reference for the power produced at node 1 by adjusting the current i_d pu, setting $i_q = 0$ pu and varying the reactive compensation at the grid connection such that the power factor at the grid connection, node 5, is as close to unity as possible, gives the results shown in table 5.2.1. The first row in the table shows the power flow at different nodes at maximum allowed power production from the wind farm had there not been any reactive power compensation in the system. The second row shows the power flow without reactive power compensation staying within the ratings of the cable. Row three presents the power flow at rated power with reactive power compensation. For a complete table of results see table A.1.1 in the appendix.

The static compensation at landfall, $Q_{3,\text{comp}}$, is set to 120 MVar for all scenarios except the first two where it is 0 Var.

Table 5.2.1: Power flow, 35 km, 50 Hz

$\mathbf{P_{1,\,ref}}$	$\mathbf{P_1}$	$\mathbf{P_2}$	$\mathbf{P_3}$	$\mathbf{P_4}$	$\mathbf{P_5}$	$\mathbf{Q_1}$	$\mathbf{Q_2}$	$\mathbf{Q_3}$	$\mathbf{Q_4}$	$\mathbf{Q_5}$	$\mathbf{Q_{3,comp}}$	$\mathbf{Q_{4,comp}}$
1	*406.1*	*403.9*	*401.0*	*395.9*	*394.4*	*3.0*	*-30.5*	*162.1*	*395.1*	*352.7*	*N/A*	*N/A*
0.128	51.9	50.5	50.2	48.3	47.1	0.4	-22.1	174.8	415.9	386.3	*N/A*	N/A
1	406.4	404.3	401.2	397.3	396.2	3.1	-29.6	-41.3	30.0	0.8	120	97
pu	(MW)					(MVar)					(MVar)	

5.2.1.1 Without Reactive Power Compensation

Without any reactive power compensation, *HR3* would not be able to operate within the physical limits of the export cable, as the reactive component would make the current too high, the RMS-values are listed in table 5.2.2 and depicted in figure 5.2.2.

What can be observed from table 5.2.1, is that from node 1 to node 2, the offshore substation transformers consume approximately 33.5 MVar reactive power. The 35 km offshore (+beach) cable produce almost 193 MVar between node 2 and 3. The 45 km onshore cable produces another 233 MVar between node 3 and 4, making the total reactive power delivered to the grid transformer, 395.1 MVar. The grid transformer consumes 47.1 MVar, giving 352.8 MVar injected into the Danish central grid. The active power generated at *HR3* is 406.1 MW, delivering 394.4 MW at the grid connection, giving a power loss of 11.7 MW, or an efficiency of $\eta = 97.1$ %.

The power factor for the power delivered to the grid in node 5, without any reactive power compensation is as low as $\cos\phi = 0.75$, as calculated in equation (5.2.1). ϕ is the angle between two vectors and can in some cases refer to the angle between the voltage vector and the vector of the total current. ϕ can also refer to the angle between the vector of the active current component, and the total current vector. As the active current vector is often aligned with the voltage vector these two usually coincide.

$$\cos\phi = \mathrm{PF} = \frac{P_5}{|S_5|} = \frac{394.4}{\sqrt{394.4^2 + 352.7^2}} = 0.75 \tag{5.2.1}$$

Since the grid transformer consumes some of the reactive power in the system the largest current is at the low voltage side of the transformer in node 4. The current components are depicted in figure 5.2.2 and the values are presented in table 5.2.2.

Table 5.2.2: Current components (RMS) of 35-km cable without reactive compensation

50 Hz				**16.7 Hz**			
$\mathbf{I_P}$ (A)	$\mathbf{I_Q}$ (A)	$\mathbf{I_{Tot}}$ (A)	ϕ (deg.)	$\mathbf{I_P}$ (A)	$\mathbf{I_Q}$ (A)	$\mathbf{I_{Tot}}$ (A)	ϕ (deg.)
817	816	1 155	45.0	843	212	869	14.1

The total current for the 50-Hz cable without any reactive compensation, is higher than the rated current of 1 099 A, as given by the cable data in table 2.1.3 in section 2.1.3.2 on

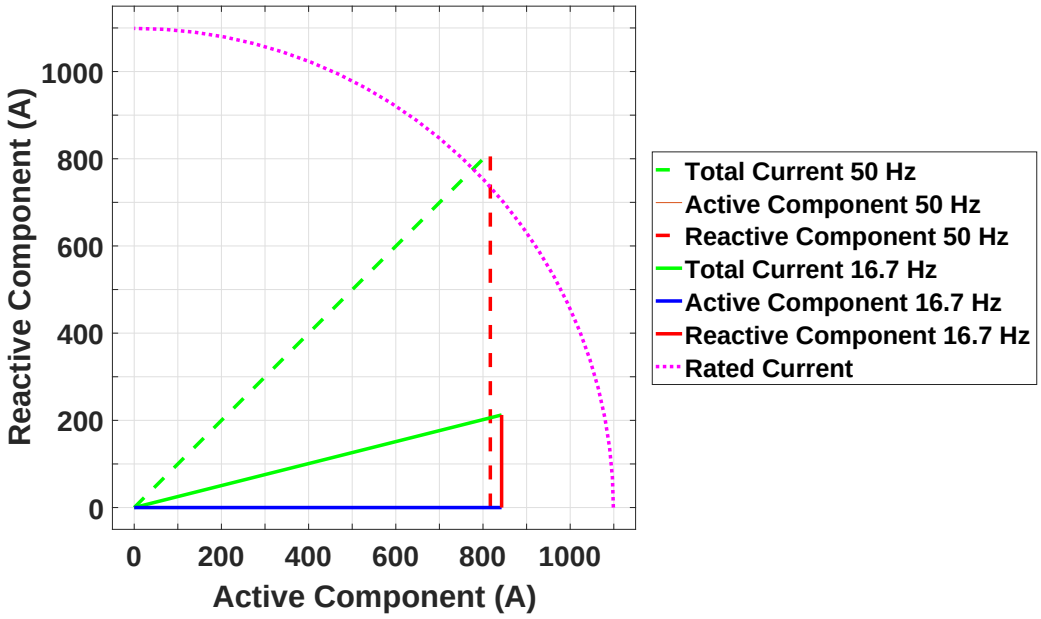

Figure 5.2.2: Active and reactive components, node 4, 35-km, 50- and 16.7 Hz, RMS-values, no compensation

page 11. It is evident that the wind farm cannot operate at maximum power production at $f = 50$ Hz, without reactive power compensation in the system.

To be able to operate within the current capability of the cable, the power production from *HR3* must be reduced to 12.8 % of the rated power. The second row of table 5.2.1, shows a maximal power production from *HR3* of $P_1 = 51.9$ MW, which is the highest permitted power production to stay below the rated current of the cable at the most critical node, node 4.

5.2.1.2 With Reactive Power Compensation

With the static reactive power compensation of 120 MVar at node 3, and 97 MVar compensation at node 4, *HR3* delivers 395.4 MW of power into the Danish central grid at node 5. The active power loss from generation in node 1, to the grid connection in node 5 is 10.2 MW, giving an overall efficiency of $\eta = 97.5$ %. The power loss is lower than without reactive power compensation due to the magnitude of the total current in the cable is lower because of a lower reactive current component.

The currents at rated power in the 35-km cable for both 50 Hz and 16.7 Hz with reactive

power compensation are presented in figure 5.2.3. The RMS-value of the current in the receiving end of the 35-km, 50-Hz cable is 898 A, or 0.82 pu. The sending end voltages are presented in figure 5.4.1, and for the 35-km, 50-Hz case, the voltage has a maximal RMS-value of 1.03 pu.

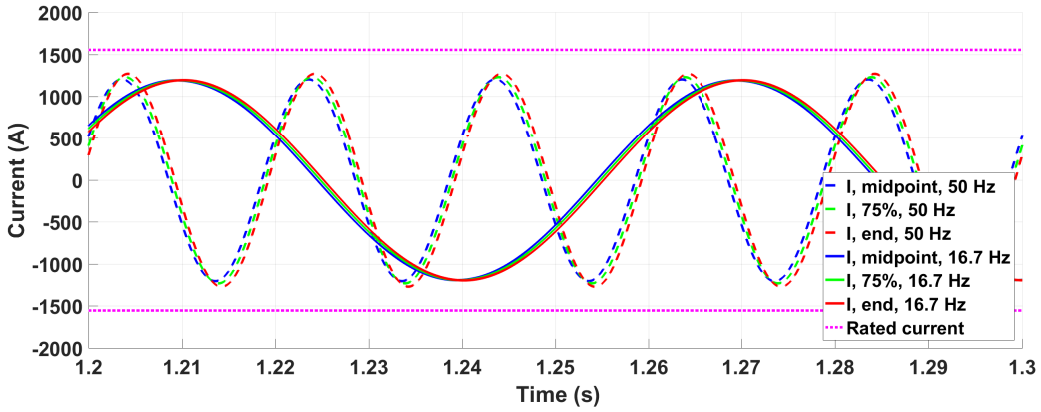

Figure 5.2.3: Current with reactive compensation, 35 km, f=50 and 16.7 Hz

5.2.2 Normal length 35 km, LFAC 16.7 Hz

Reducing the frequency to $f = 16.7$ Hz, gives the results in table 5.2.3. First row indicates the power flow without reactive compensation. For complete results see table A.1.2 in the appendix.

The static reactive compensation at node 3 is reduced to 1/3 of the rating for 50 Hz operation, and is for the 16.7 Hz scenario set to 40 MVar, except for the first row, where it is zero.

Table 5.2.3: Power flow, 35 km, LFAC 16.7 Hz

$\mathbf{P_{1,\,ref}}$	$\mathbf{P_1}$	$\mathbf{P_2}$	$\mathbf{P_3}$	$\mathbf{P_4}$	$\mathbf{P_5}$	$\mathbf{Q_1}$	$\mathbf{Q_2}$	$\mathbf{Q_3}$	$\mathbf{Q_4}$	$\mathbf{Q_5}$	$\mathbf{Q_{3,comp}}$	$\mathbf{Q_{4,comp}}$
1	*405.9*	*403.7*	*400.8*	*397.0*	*395.9*	*1.0*	*-31.6*	*26.8*	*100.1*	*70.3*	*N/A*	*N/A*
1	405.6	403.5	400.4	396.6	395.5	1.1	-31.4	-35.49	30.7	1.6	40	4
pu	(MW)					(MVar)					(MVar)	

For the case where LFAC is used, $f = 16.7$ Hz, the current in node 4 is 1 074.5 A and hence stays within the current capability of the cable (1 099 A) even without any reactive power compensation in the system.

The power factor delivered to the grid in node 5 is in this case $\cos\phi = \dfrac{395.9 \text{ MW}}{402.0 \text{ MVA}} = 0.98$.

With static reactive power compensation of 40 MVar at landfall, node 3, the variable reactive power compensation needed in node 4, $Q_{4,\text{comp}}$ is below 27 MVar for all scenarios to keep the power factor as close to unity as possible.

5.2.3 Comparing LFAC with ordinary AC for the Case of HR3, 35 km cable

It is apparent that reducing the frequency from 50 Hz to 16.7 Hz would exclude the need for reactive power compensation in case of the data given for and simulations done for *Horns Rev 3* with a cable length of 35 km.

The comparison of the different scenarios without reactive power compensation for the 35-km cable, operating at full capacity of the wind farm, are shown in figure 5.2.4.

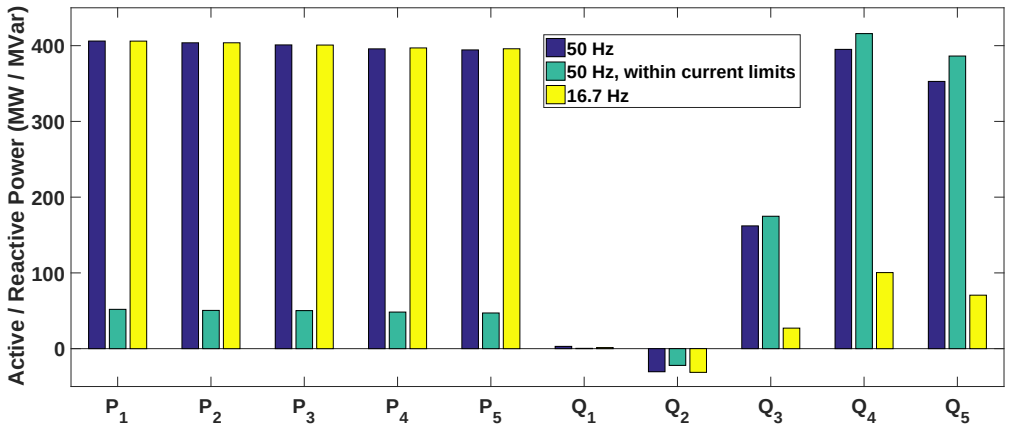

Figure 5.2.4: Power flow in 35 km cable without reactive power compensation, 50 Hz and LFAC

5.3 Offshore Cable Length 100km

With an offshore cable length of 100km the limits for the reactive power compensation of the real case presented in section 5.2 for *HR3* are neglected. The reactive power compensation needed in node 3 to keep the current below the rated value in node 3, and the reactive power compensation needed in node 4 for delivering at unity power factor in node 5 is used. This is a way to quantify the reactive power compensation needed under the condition of increased cable length.

5.3.1 Offshore Cable Length 100 km, 50 Hz

First row of table 5.3.1 shows the power flow without reactive compensation. At this scenario the current in node 4 would be as high as 2 443 A, which is more than double the rated cable current. The grid transformer between node 4 and node 5 has a rating of 450 MVA, which is exceeded if there is no reactive power compensation in the system. It is not possible to stay below the rated cable current, operating at normal frequency, for any power production from the wind farm, without reactive compensation.

With reactive power compensation of 225 MVar at node 3 and 220 MVar at node 4, the system delivers 375.8 MW of active power at unity power factor to the grid connection in node 5, giving a total efficiency of $\eta = 92.4$ %. The current in the cable is depicted in figure 5.3.1.

Table 5.3.1: Power flow, 100 km, 50 Hz

$\mathbf{P_{1,\,ref}}$	$\mathbf{P_1}$	$\mathbf{P_2}$	$\mathbf{P_3}$	$\mathbf{P_4}$	$\mathbf{P_5}$	$\mathbf{Q_1}$	$\mathbf{Q_2}$	$\mathbf{Q_3}$	$\mathbf{Q_4}$	$\mathbf{Q_5}$	$\mathbf{Q_{3,comp}}$	$\mathbf{Q_{4,comp}}$
1	*406.5*	*404.1*	*391.9*	*378.2*	*375.8*	*3.0*	*-33.6*	*615.7*	*850.8*	*763.3*	*N/A*	*N/A*
1	405.8	403.6	391.5	386.4	385.3	3.1	-30.7	143.7	29.0	0.7	225	220
pu	(MW)					(MVar)					(MVar)	

However, as depicted in figure 5.3.1 the current at the recieving end of the cable is too high, and it is not possible to operate at fully rated power with a 100-km cable at 50 Hz, even with reactive power compensation at the onshore end of the cable. The dotted magenta-colored line in figure 5.3.1 indicates the amplitude of the rated current of the cable, $\hat{I} = \sqrt{2} \cdot I_{\text{RMS}} = \sqrt{2} \cdot 1\ 099\ \text{A} = 1\ 554.2\ \text{A}$.

The blue lines are at the midpoint of the cable, the green is at 75 % cable length, while the red is at the end of the cable. At 75 % of the cable length, the current is $I_{\text{RMS}} = 1\ 118$ A, and at the end of the offshore cable it has reached 1 326 A, which are both higher than the rated current of 1 099 A.

5.3.2 Offshore Cable Length 100 km, LFAC 16.7 Hz

Having a cable length of 100 km and reducing the frequency to 16.7 Hz gives the results in table 5.3.2. For complete results at lower power production, see table A.1.4 in the appendix.

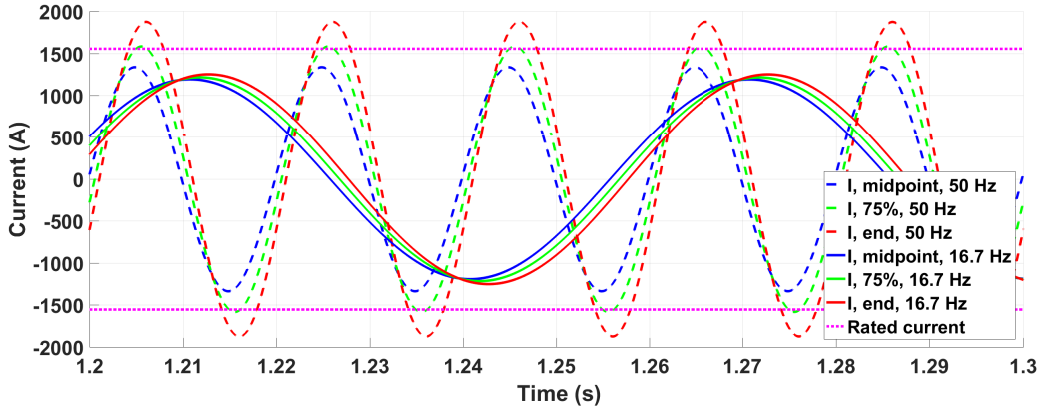

Figure 5.3.1: Current with reactive compensation, 100 km, f=50 and 16.7 Hz

Without any reactive power compensation, the current in node 4 is 1 172 A and is only 6.6 % above the rated current of 1 099 A.

With a reactive power compensation of $Q_{3,\text{comp}} = Q_{4,\text{comp}} = 59$ MVar, the wind farm can deliver 389.6 MW to the grid in node 5, with a total active power loss of 15.8 MW, equivalent to an overall efficiency of $\eta = 96.1$ %.

The current in the cable at rated power production with reactive power compensation was depicted in figure 5.3.1, and has an RMS value of 885 A.

Table 5.3.2: Power flow, 100 km, LFAC 16.7 Hz

$\mathbf{P_{1,\,ref}}$	$\mathbf{P_1}$	$\mathbf{P_2}$	$\mathbf{P_3}$	$\mathbf{P_4}$	$\mathbf{P_5}$	$\mathbf{Q_1}$	$\mathbf{Q_2}$	$\mathbf{Q_3}$	$\mathbf{Q_4}$	$\mathbf{Q_5}$	$\mathbf{Q_{3,comp}}$	$\mathbf{Q_{4,comp}}$
1	*406.7*	*404.4*	*396.3*	*392.0*	*390.8*	*1.0*	*-32.2*	*142.5*	*217.2*	*184.6*	*N/A*	*N/A*
1	405.9	403.6	394.9	391.1	390.0	1.0	-31.7	44.9	28.2	-0.5	59	59
pu			(MW)					(MVar)			(MVar)	

5.4 Offshore Cable Length 200km

A distance of 200 km would be the longest AC link in the world, and with a rated power of several hundred megawatts and a high voltage rating it by far outnumber the next connections on the list.

At present, the longest AC-cable in the world is the 164 km *Martin Linge* cable, connecting the offshore oil- and gas platform to power from shore. It is designed for 55 MW at a voltage of 100 kV and has reactive power compensation of 20-130 MVar at the onshore

end of the cable [10].

The voltages in the sending end of the cable for different cable lengths and frequencies are depicted in figure 5.4.1.

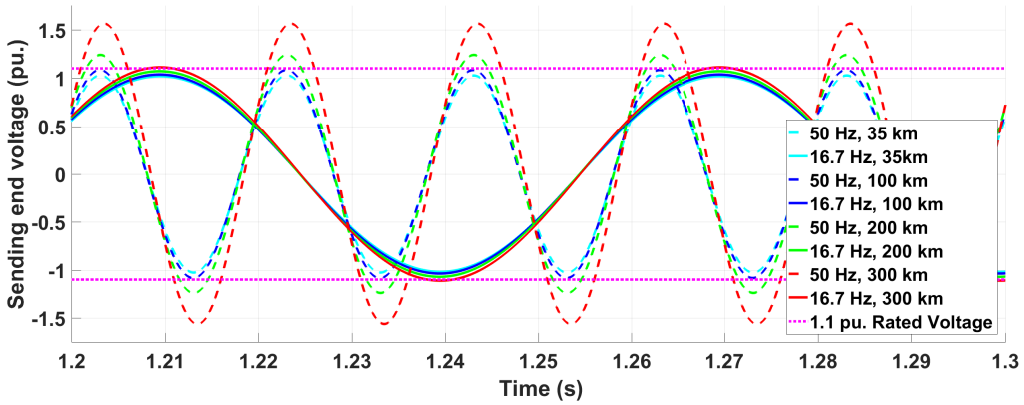

Figure 5.4.1: Sending end voltage at rated power, 50 Hz and LFAC, 35-, 100-, 200 and 300 km

5.4.1 Offshore Cable Length 200 km, 50 Hz

It doesn't make much sense to investigate how the wind farm would operate at $f = 50$ Hz with an offshore cable length of 200 km (making the total cable length 244.8 km) without any reactive power compensation. But the simulation in the first row of table 5.4.1 is done in order to serve as an example of how high the reactive power in the system becomes. For a complete table of the power flow at lower power production see table A.1.6 in the appendix.

Table 5.4.1: Power flow, 200 km, 50 Hz

$\mathbf{P_{1,\,ref}}$	$\mathbf{P_1}$	$\mathbf{P_2}$	$\mathbf{P_3}$	$\mathbf{P_4}$	$\mathbf{P_5}$	$\mathbf{Q_1}$	$\mathbf{Q_2}$	$\mathbf{Q_3}$	$\mathbf{Q_4}$	$\mathbf{Q_5}$	$\mathbf{Q_{3,comp}}$	$\mathbf{Q_{4,comp}}$
1	*406.2*	*402.9*	*315.4*	*256.7*	*249.7*	*3.0*	*-47.7*	*1 786*	*1 956*	*1 658*	*N/A*	*N/A*
1	405.7	403.2	340.0	334.6	333.6	3.0	-35.3	233.4	25.4	0.8	580	282
pu	(MW)					(MVar)					(MVar)	

When the wind farm has a power production of 403.1 MW and reactive compensation of $Q_{3,\text{comp}}$ 580 MVar and $Q_{4,\text{comp}}$ 282 MVar, the total power loss is 71.9 MW, giving an efficiency of $\eta = 82.2$ %. However, the current in the receiving end of the cable is too high, with an RMS value of 2 515 A, as depicted in figure 5.4.2. And the sending end

voltage, depicted in figure 5.4.1, is too high, with a value of 1.24 pu. Having a 200-km cable operating at 50 Hz is not possible at a voltage level of 220 kV with only reactive power compensation at the receiving end of the cable.

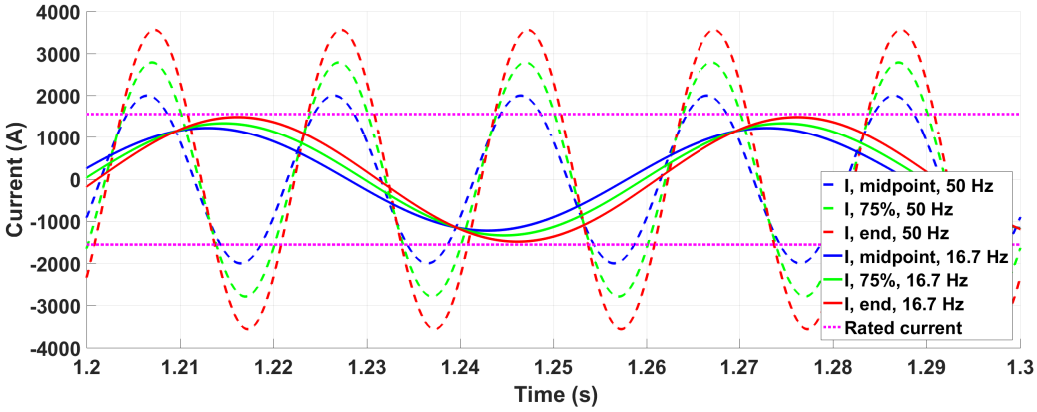

Figure 5.4.2: Current with reactive compensation, 200 km, f=50 and 16.7 Hz

5.4.2 Offshore Cable Length 200 km, LFAC 16.7 Hz

The power flow without reactive compensation is presented in the first row of table 5.4.2, while the second row gives the power flow with reactive compensation. The complete table showing power flows at lower power production is placed in table A.1.6 in the appendix.

Without any reactive compensation, the apparent power at node 4 is 564.4 MVA, which gives a current of 1 481 A, or 135 % of the rated value. Without any reactive power compensation in the system, it is not possible to stay within the rated current limit for any amount of active power production at the wind farm.

Staying within the rated current at node 3 and unity power factor at node 5, the reactive power compensation needed is $Q_{3,\text{comp}} = 100$ MVar and $Q_{4,\text{comp}} = 135$ MVar. Giving a total efficiency of $\eta = 93.5$ %.

When reactive power compensation is used, both voltage and current of the offshore cable stay within the rated limits. The largest RMS-current in the cable is 1 056 A at maximal power production, which is depicted in figure 5.4.2. And the voltage in the sending end is 1.07 pu, as depicted in figure 5.4.1.

Table 5.4.2: Power flow, 200 km, LFAC 16.7 Hz

$\mathbf{P_{1,\,ref}}$	$\mathbf{P_1}$	$\mathbf{P_2}$	$\mathbf{P_3}$	$\mathbf{P_4}$	$\mathbf{P_5}$	$\mathbf{Q_1}$	$\mathbf{Q_2}$	$\mathbf{Q_3}$	$\mathbf{Q_4}$	$\mathbf{Q_5}$	$\mathbf{Q_{3,comp}}$	$\mathbf{Q_{4,comp}}$
1	*405.7*	*403.3*	*384.9*	*378.5*	*377.1*	*1.0*	*-33.3*	*343.5*	*419.4*	*376.6*	*N/A*	*N/A*
1	405.4	403.1	383.9	379.5	378.5	1.0	-32.3	160.2	28.6	0.8	100	135
pu	(MW)					(MVar)					(MVar)	

5.5 Offshore Cable Length 300km

5.5.1 Offshore Cable Length 300km, 50 Hz

The case using a frequency of 50 Hz is not simulated without any reactive compensation. The results at rated power are shown in table 5.5.1, while the complete table of power flows is presented in table A.1.7 in the appendix.

With reactive power compensation of $Q_{3,\text{comp}} = 1.065$ GVar and $Q_{4,\text{comp}} = 400$ MVar, the wind farm delivers 121.5 MW to the grid in node 5. Giving an overall efficiency of $\eta = 30.0$ %. However both voltage (figure 5.4.1) and current (figure 5.5.1) of the cable exceeds the allowed limits, and operation with reactive power compensation only from one side of the cable is not possible.

Table 5.5.1: Power flow, 300 km, 50 Hz

$\mathbf{P_{1,\,ref}}$	$\mathbf{P_1}$	$\mathbf{P_2}$	$\mathbf{P_3}$	$\mathbf{P_4}$	$\mathbf{P_5}$	$\mathbf{Q_1}$	$\mathbf{Q_2}$	$\mathbf{Q_3}$	$\mathbf{Q_4}$	$\mathbf{Q_5}$	$\mathbf{Q_{3,comp}}$	$\mathbf{Q_{4,comp}}$
1	405.4	402.0	128.7	122.3	121.5	3.0	-49.9	395.8	10.0	-5.0	1 065	400
pu	(MW)					(MVar)					(MVar)	

The voltage at rated power in the sending end is 1.56 pu at 50 Hz when the cable is 300 km long, see figure 5.4.1. The RMS-current in the receiving end is 4 391 A, approximately four times the rated current of the cable, see figure 5.5.1.

5.5.2 Offshore Cable Length 300km, LFAC 16.7 Hz

The first row of table 5.5.2 shows the power flow at 16.7 Hz for the 300-km cable when there is no reactive power compensation in the system. This mode of operation far exceeds the current ratings of the cable, but serves as an illustration.

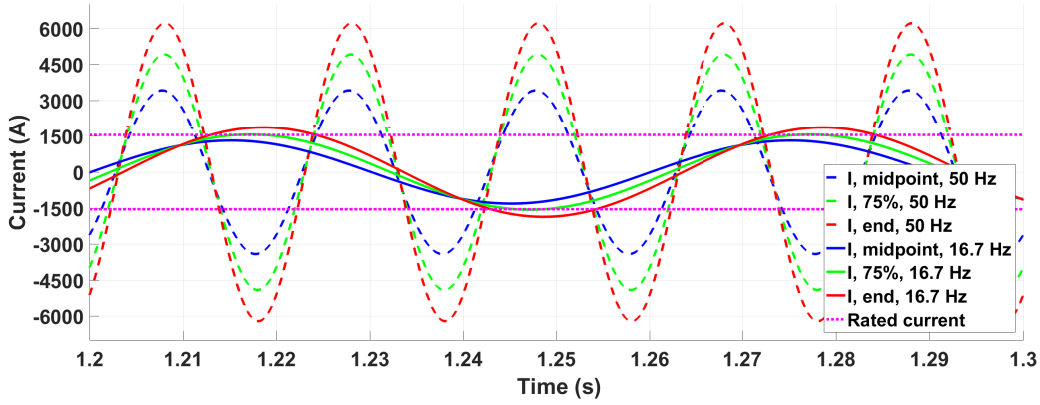

Figure 5.5.1: Current with reactive compensation, 300 km, f=50 and 16.7 Hz

With reactive power compensation of $Q_{3,\text{comp}} = 196$ MVar and $Q_{4,\text{comp}} = 165$ MVar, the active power loss is 43.7 MW, giving an efficiency of $\eta = 89.1$ %.

The voltage at the sending end of the cable is 1.11 pu at rated power, as seen by figure 5.4.1. The RMS-current is 1 113 A at 75 % of the cable length, while it has reached 1 323 A at the receiving end, exceeding the limits of the rated current, 1 099 A.

Table 5.5.2: Power flow, 300 km, LFAC 16.7 Hz

$\mathbf{P_{1,\text{ref}}}$	$\mathbf{P_1}$	$\mathbf{P_2}$	$\mathbf{P_3}$	$\mathbf{P_4}$	$\mathbf{P_5}$	$\mathbf{Q_1}$	$\mathbf{Q_2}$	$\mathbf{Q_3}$	$\mathbf{Q_4}$	$\mathbf{Q_5}$	$\mathbf{Q_{3,\text{comp}}}$	$\mathbf{Q_{4,\text{comp}}}$
1	*406.6*	*404.0*	*368.1*	*357.3*	*355.8*	*1.0*	*-35.2*	*578.2*	*653.8*	*591.3*	*N/A*	*N/A*
1	404.7	402.2	366.3	361.8	360.7	1.0	-33.2	203.6	26.8	0.3	196	165
pu			(MW)					(MVar)			(MVar)	

5.6 Transformers at LFAC

The following sections are elaborated based on inputs provided by *ABB* in Finland, which to some extent coincide with the findings made in research papers on the topic of LFAC transformers.

5.6.1 Wind Turbine Transformer

The transformer in the wind turbine used for the *V164-8.0 MW* will according to *ABB* [41], who is the producer, have the following relations for the LFAC components when com-

pared to the normal 50-Hz component. The actual numbers are confidential, but table 5.6.1 gives the relative size to the 50-Hz component as an indication.

Table 5.6.1: Relative parameters LFAC vs. 50-Hz, *V164*-transformer [41]

	% of 50-Hz values
Weight	187
Length	117.6
Width	113.4
Height	111.4
Volume	148.6
$\mathbf{P}_{\text{loss, no-load}}$	58.3
$\mathbf{P}_{\text{loss, full-load}}$	163.6

The by far largest of the two losses, the full-load loss, is below 1 % of the rated MVA of the transformer, and for LFAC operation this is increased by more than 60 %.

5.6.2 Offshore Substation Transformer

For the offshore substation transformers, the actual numbers are confidential, but the relative change for LFAC components compared to those of 50-Hz gives the relationship in table 5.6.2.

Table 5.6.2: Relative parameters LFAC vs. 50-Hz, substation transformer [41]

	% of 50-Hz values
Weight	258
$\mathbf{P}_{\text{loss, no-load}}$	52.9
$\mathbf{P}_{\text{loss, full-load}}$	240.0

The by far largest of the two losses, the full-load loss, is below 1 % of the rated MVA of the transformer. For the LFAC substation transformer this is more than doubled compared to an equivalent 50-Hz transformer.

5.7 Reactive Compensation at LFAC

It has not been successful to uncover many details about the reactive power compensation, but *ABB* predicts [41] that for instance a 120 MVar reactor designed for 50-Hz operation would have about the same physical dimensions and weight, and the same power loss as a reactor of 40 MVar operating at 16.7 Hz. It is suggested that this also applies to reactors with other ratings.

Chapter 6

Discussion

The consequences and possible implications of the findings in chapter 5, results, are discussed in this chapter.

6.1 Comparison of normal AC vs. LFAC

6.1.1 Current, Power Loss and Voltage

In general, it can be observed that for the scenarios operating at a reduced frequency the magnitude of current in the offshore cable is substantially reduced. This is due to a lower reactive current component because of lower reactive power production at reduced frequency, as expected by the relationship presented in equation (3.5.2).

The increased magnitude of the current through the cable gives rise to a higher power loss for the cable operating under normal frequency, compared to that of LFAC operation. The resistive power loss in the cable is given by $P_{\text{loss}} = R_{\text{cable}} \cdot |I|^2$, hence the active power loss is higher if the current in the cable is higher. This affects the efficiency of the system, where a higher resistive power loss consequently leads to a lower efficiency.

The efficiency at different cable length and frequencies are given in table 6.1.1, and illustrated in figure 6.1.1.

What increases the efficiencies so substantially by reducing the frequency from 50 Hz to 16.7 Hz is as mentioned that the resistive power loss in the cable is much lower when the

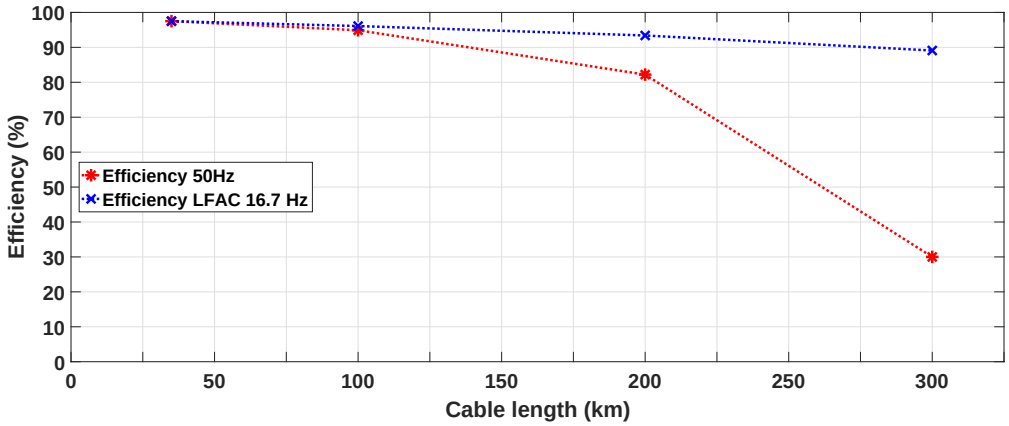

Figure 6.1.1: Power system efficiency at different cable lengths and frequencies with reactive compensation

magnitude of the total current is reduced.

Table 6.1.1: Efficiency at different cable lengths and frequencies

	50 Hz					16.7 Hz				
Length (km)	$\mathbf{P_1}$ (MW)	$\mathbf{P_{loss}}$ (MW)	$\mathbf{P_5}$ (MW)	η (%)	$\mathbf{\Sigma Q_{comp}}$ (MVar)	$\mathbf{P_1}$ (MW)	$\mathbf{P_{loss}}$ (MW)	$\mathbf{P_5}$ (MW)	η (%)	$\mathbf{\Sigma Q_{comp}}$ (MVar)
35	406.4	10.2	396.2	97.5	217	405.6	10.1	395.5	97.5	44
100	405.8	20.5	385.3	94.9	445	405.9	15.9	390.0	96.1	118
200	405.7	72.1	333.6	82.2	962	405.4	26.9	378.5	93.4	235
300	405.4	283.9	121.5	30.0	1 465	404.7	44.0	360.7	89.1	261

High resistive power losses in the cable also present issues regarding cable voltage. As presented in the plot of sending end cable voltage at different lengths and frequencies, figure 5.4.1, the voltage was substantially higher at higher frequency and long cable lengths. This can be explained by rewriting *Ohm's law*, $V = Z \cdot I$, resulting in equation (6.1.1), where V is the voltage across a component, I is the current through it, and Z is the impedance of the component. The total current in the cable, I_{Tot}, and the angle, ϕ, between the active current component, I_{P}, and the total current, are presented in table 6.1.2. R' and L' are the resistance and inductance per unit length of cable.

$$\Delta V_{\text{cable}} \approx |I_{\text{Tot}}| \cdot l_{\text{cable}} \cdot \Big(R' \cdot \cos(\phi) + 2\pi \cdot f \cdot L' \cdot \sin(\phi)\Big) \tag{6.1.1}$$

Equation (6.1.1) is an approximated formula stating that the voltage drop of the power cable is related to the magnitude of the current through it, hence a higher current results

in a higher power loss and a higher voltage drop across the cable. The expression for the approximated voltage drop also contains a component proportional to the frequency. Higher current and frequency makes the sending end voltage in node 2, at the offshore end of the cable, higher to be able to deliver power at rated voltage onshore.

A large current in the offshore cable, which is the case at normal frequency, penalizes both the power loss in the cable, and the operating voltage. The increased voltage is also responsible for a higher reactive power production in the cable in the first place, as the reactive power production is proportional to the square of the voltage.

The current limits of the cable, makes operating at 50 Hz impossible at rated power, for every distance examined, except at 35 km, when there is reactive power compensation only in the receiving end of the cable.

When the frequency is reduced to LFAC, 16.7 Hz, with reactive compensation from the onshore end, the rated current is not exceeded for any of the simulated cable lengths, except for the 300-km cable. As mentioned in section 5.4 the longest AC-link in the world is 164 km, and operates at a much lower rated power and voltage.

The limits for the voltage shown in figure 6.1.2 (enlarged view, see figure A.3.1 in the appendix) is the amplitude of the RMS-equivalent voltage rating of the cable. The sending end voltage of the cable is above the limit of 1.1 pu for 50 Hz at both 200- and 300 km. For 16.7 Hz it exceeds the limit for 300 km at rated power, but with a maximal value of only 1.11 pu at rated power, reducing the power output slightly would result in a voltage level below the 1.1 pu limit. However, 1.11 pu should not be a problem for the cable as *IEC62067:2011* states that a 220-kV cable should be designed for a maximal permanent operating voltage of 245 kV, or 1.114 pu.

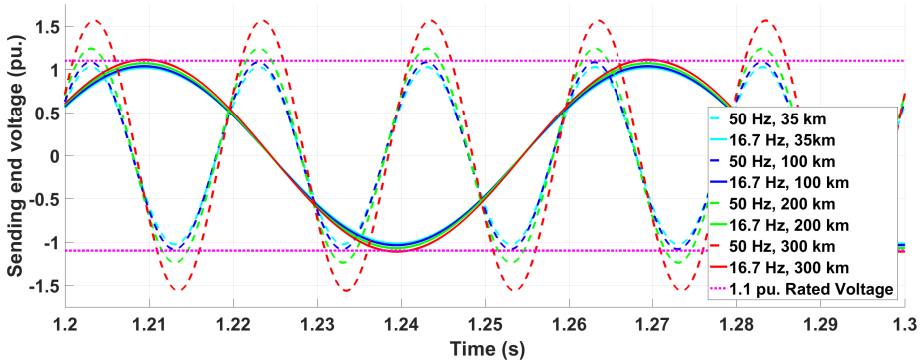

Figure 6.1.2: Cable voltage at node 2, sending end, pu.

6.1.1.1 Reactive Current Component

As previously stated it is the reactive current component that gives problems regarding the current rating of the power cable. In figure 6.1.3 the active- and reactive components (real and imaginary axis) of the current in the receiving end of the 200-km cable with reactive compensation, as listed in table 5.4.1 and table 5.4.2, are presented in RMS-values. What can be observed is that for the normal-frequency case, the reactive component (y-axis) is making the total current in the cable exceed the rated value. For the LFAC case the reactive component is much lower, and the current stays within the cable ratings.

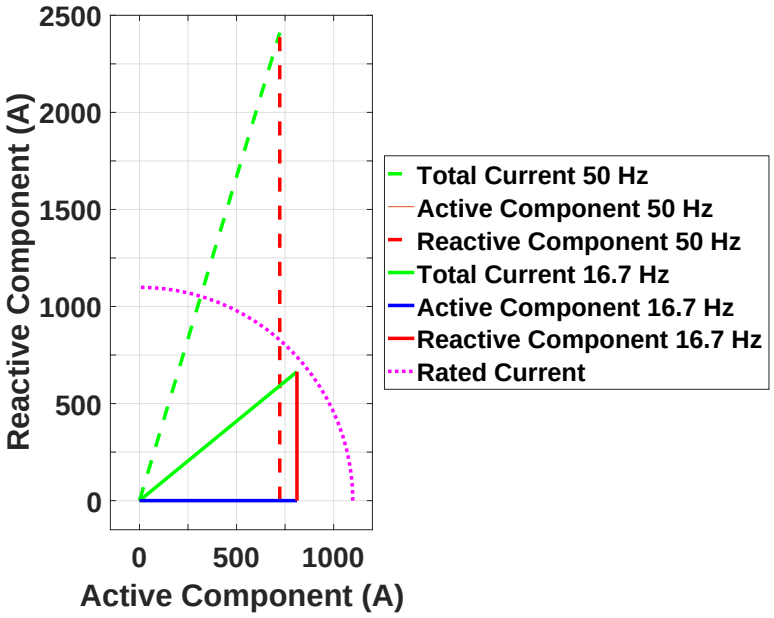

Figure 6.1.3: Active and reactive components, receiving end, 200 km, 50- and 16.7 Hz, RMS-values

The angle between the active component and the total current-vector is denoted by ϕ. The active component is used as a reference and is aligned with the voltage at the point of measurement. The value of the different current components along with the angle between them are presented in table 6.1.2.

6.1.2 Offshore Reactive Power Compensation, $Q_{2,\,\mathrm{comp}}$

It has been shown that it is not possible to operate the system with a cable length of 300 km only with reactive power compensation from the onshore end of the cable. If also

Table 6.1.2: Current components (RMS) at different lengths and frequencies with reactive compensation

	50 Hz				16.7 Hz			
Length (km)	$\mathbf{I_P}$ (A)	$\mathbf{I_Q}$ (A)	$\mathbf{I_{Tot}}$ (A)	ϕ (deg.)	$\mathbf{I_P}$ (A)	$\mathbf{I_Q}$ (A)	$\mathbf{I_{Tot}}$ (A)	ϕ (deg.)
35	844	305	897	19.9	848	55	850	3.7
100	817	1 043	1 325	51.9	836	287	884	18.9
200	723	2 411	2 517	73.3	811	664	1 048	39.3
300	313	4 383	4 394	85.9	779	1 070	1 324	53.9

reactive compensation offshore is introduced, the picture might change.

To keep the current within the limits at rated power production, the 300-km cable need an offshore reactive power compensation of $Q_{2,\text{comp}} = 82$ MVar, while $Q_{3,\text{comp}} = 125$ MVar and $Q_{4,\text{comp}} = 140$ MVar. The current for the 300-km cable with compensation only from the onshore end of the cable and with reactive compensation from both ends is depicted in figure 6.1.4, and the power flows with reactive power compensation offshore are presented in table 6.1.3. The complete table at lower power production is presented in table A.1.9 in the appendix.

Table 6.1.3: Power flow, 300 km, LFAC 16.7 Hz with reactive compensation offshore

$\mathbf{P_{1,\text{ref}}}$	$\mathbf{P_1}$	$\mathbf{P_2}$	$\mathbf{P_3}$	$\mathbf{P_4}$	$\mathbf{P_5}$	$\mathbf{Q_1}$	$\mathbf{Q_2}$	$\mathbf{Q_3}$	$\mathbf{Q_4}$	$\mathbf{Q_5}$	$\mathbf{Q_{2,\text{comp}}}$	$\mathbf{Q_{3,\text{comp}}}$	$\mathbf{Q_{4,\text{comp}}}$
1	405.9	403.7	376.8	372.6	371.5	1.0	-178.9	162.7	23.8	-3.5	82	125	140
pu	(MW)					(MVar)					(MVar)		

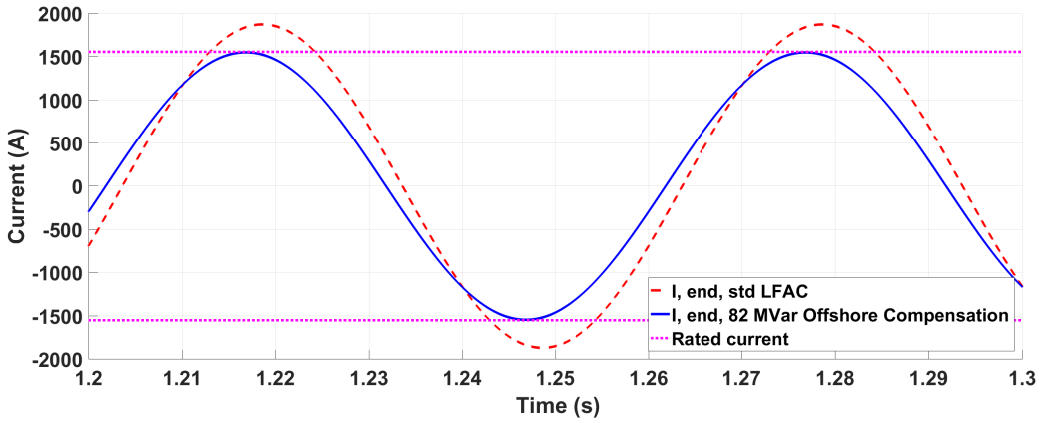

Figure 6.1.4: Phase current with reactive compensation from onshore end (red) and from both ends (blue), 300 km, LFAC

Without reactive compensation offshore, the RMS current is 1 326 A, while with an offshore reactive compensation of $Q_{2,\text{comp}} = 82$ MVar the current is kept below the rated limit of the cable, 1 099 A.

With reactive power compensation offshore, the efficiency of the system would be increased from 89.1 %, with only reactive compensation onshore (but violating the current and voltage limits) to 91.5 %, as calculated in equation (6.1.2).

$$\eta = \frac{\text{Power output}}{\text{Power input}} = \frac{P_5}{P_1} = \frac{371.5 \text{ MW}}{405.9 \text{ MW}} = 91.5 \text{ \%} \tag{6.1.2}$$

Reduced operating frequency opens the possibility for reaching distances using AC-cables, that has previously been out of reach. LFAC still have a need for reactive power compensation, but it is technically possible to apply such solutions to long cable lengths, for high power- and voltage ratings.

Simplifying the topologies due to possible exclusion of the need for reactive power compensation is one of the key benefits for LFAC-systems. Therefore, it might seem strange to suggest an even more complicated topology including also reactive power compensation offshore, but as presented this opens the possibility for reaching distances that would be difficult/impossible to reach using higher frequencies.

6.2 Size and Weight of Transformers and Reactive Compensation

The advantages presented of lowering the operational frequency of the offshore power grid comes at a cost. As mentioned in section 3.7.4 on page 29, reduced frequency consequently leads to increased physical dimensions of the transformer and devices used for reactive compensation.

The size and weight of the different components operating at LFAC are not investigated in detail, but previous research has shown that the physical size of a component is not necessarily directly proportional to the operating frequency. Research by both *Erlich et al.* [23] and *Wyllie et al.* [36] suggests that reducing the frequency to 1/3 of the normal frequency would approximately only double the size and weight of the transformer.

There are some divergences between the findings from the research papers discussing size and weight of LFAC transformers and the information given by *ABB* regarding the substation transformers. *ABB* produce and design transformers for a wide range of power system applications, and even though their estimates are higher than the research papers, this is a company that have been producing power transformers for more than a century, which should be taken into account.

6.2.1 Wind Turbine Transformer

The findings from *ABB* in section 5.6 suggests that the volume of the transformer in each wind turbine would be approximately 150 % for LFAC 16.7 Hz components compared to the corresponding 50-Hz component. The weight would almost be doubled, equivalent to 187 % of the weight of the corresponding normal-frequency component.

Wyllie et al. [36] shows that their 8 MVA transformer for individual WTGs would have a weight of approximately 208 % for LFAC operation compared to that of 50 Hz. And the volume would also be more than doubled, equivalent to 207 %.

These numbers cannot be compared one to one as the ratings are different, but even though these numbers are not exactly the same, they imply that reducing the frequency to 1/3 of the original design, would not lead to a tripling of the transformer weight for the transformer in the individual wind turbine.

6.2.2 Offshore Substation Transformer

The findings from *ABB* regarding the LFAC substation transformers, suggest that they would have a weight about 2.58 times that of the equivalent 50-Hz component.

Wyllie et al. [36] suggests that the two different designs, the tall design, increasing the number of turns in the transformer, and the wide design, increasing the area of the transformer core, would have a weight of 1.77 and 2.88 times that of the 50-Hz reference. Figure 3.7.2, in section 3.7.4 on page 31, illustrates the difference between the wide and tall design.

Again the numbers cannot be compared one to one, as the basis is not the same, but the numbers shows that the wide design by *Wyllie et al.* is not too far from that of *ABB*.

The numbers suggests that the reduction in frequency is not directly proportional to the increase in weight.

6.3 Other Methods for Reducing Reactive Power Production

Using for instance transformers equipped with tap-changers enables reducing the cable voltage if the system operates below rated power. This would increase the current in the cable, but ensuring that the current is below the rated value a reduction in cable voltage would lead to a lower reactive power production and hence a lower reactive component of the total current in the cable. One method for optimizing the operating point of long HVAC cables is suggested by *Vrana* and *Mo*, where a reduction in the voltage of a power cable would increase the length for power transfer substantially [42]. This can be done by many different means, but using tap changers is an relatively easy method that contributes towards reducing the reactive power production in power cables.

Chapter 7

Conclusion and Further Work

The thesis concludes based on the simulations done for the different scenarios, inputs from *ABB* and discussions of the consequences on the suggested technical solutions.

7.1 Conclusion

The thesis has investigated different scenarios for low frequency AC-transmission based on a real offshore wind farm, *Horns Rev 3*, being built outside the Danish coast. The simulations done are based on data from the operator of *HR3*, *Vattenfall* and the Dansih transmission system operator, *Energinet*. Additional data on transformers and reactors have been provided by *ABB*.

Using LFAC for the realistic case of *Horns Rev 3*, with an offshore cable length of 35 km, would exclude the need for reactive power compensation in the power system.

The simulations done has proved that, for an offshore wind farm with similar ratings as *HR3* would, with reactive compensation from the onshore end only, be able to operate at a distance of 200 km from shore. This would be longer than the 164 km cable that is presently the world's longest AC cable.

With offshore reactive power compensation an equally rated wind farm as *HR3* would be able to operate at rated power of 406.7 MW at a distance of 300 km from shore, making the cable by far the longest AC-link in the world. However, the weight of the substation transformers for LFAC would be up to 2.7 times that of the 50-Hz equivalent, and in

addition having the need for reactive compensation offshore, might imply that HVDC could be a more competitive and flexible option, but this again depends on actual costs.

For all cases, regardless of offshore compensation. The reduction in frequency would lead to a weight for the offshore substation transformer that would be somewhere in the range of 1.8 to 2.7 times the weight of the 50-Hz reference, where the upper estimate is from *ABB*, a company with long history producing power transformers. As weight and size are issues of great importance when considering installations offshore, this will be an argument against using LFAC.

The thesis has not taken into account the costs of the different components, and this would need to be considered to conclude whether or not to pursue a LFAC solution for a specific power system.

7.2 Further Work

Investigations regarding size, weight and costs of the transformers and reactive power compensators would be needed to evaluate whether to implement LFAC for use at a specific offshore wind farm.

Appendix A

Power Flows, Cable Voltage and Currents

A.1 Power Flows

This section presents complete tables of the power flow in the different nodes ranging from $P_{1,\,\mathrm{ref}} = 1$ pu to zero power production.

A.1.1 35 km

Table A.1.1 has 120 MVar reactive power compensation in node 3.

Table A.1.1: Complete power flow, *HR3 Reference Case*, 35 km, 50 Hz

$\mathbf{P_{1,\,ref}}$	$\mathbf{P_1}$	$\mathbf{P_2}$	$\mathbf{P_3}$	$\mathbf{P_4}$	$\mathbf{P_5}$	$\mathbf{Q_1}$	$\mathbf{Q_2}$	$\mathbf{Q_3}$	$\mathbf{Q_4}$	$\mathbf{Q_5}$	$\mathbf{Q_{3,comp}}$	$\mathbf{Q_{4,comp}}$
1	*406.1*	*403.9*	*401.0*	*395.9*	*394.4*	*3.0*	*-30.5*	*162.1*	*395.1*	*352.7*	*N/A*	*N/A*
0.128	51.9	50.5	50.2	48.3	47.1	0.4	-22.1	174.8	415.9	386.3	N/A	N/A
1	406.4	404.3	401.2	397.3	396.2	3.1	-29.6	-41.3	30.0	0.8	120	97
0.8	325.1	323.2	321.2	318.7	317.7	2.4	-25.9	-34.9	24.6	1.0	120	107
0.6	242.9	241.3	240.1	238.6	237.7	1.8	-23.1	-30.0	18.5	-0.7	120	116
0.4	162.7	161.3	160.7	159.9	159.1	0.2	-21.2	-26.7	15.9	-0.2	120	121
0.2	80.8	79.5	79.2	78.9	78.1	0.6	-20.2	-25.0	14.0	-0.1	120	124
pu			(MW)					(MVar)			(MVar)	

Table A.1.2 has a static 40 MVar reactive power compensation in node 3.

Table A.1.2: Complete power flow, 35 km, LFAC 16.7 Hz

$P_{1,\,ref}$	P_1	P_2	P_3	P_4	P_5	Q_1	Q_2	Q_3	Q_4	Q_5	$Q_{3,comp}$	$Q_{4,comp}$
1	*405.9*	*403.7*	*400.8*	*397.0*	*395.9*	*1.0*	*-31.6*	*26.8*	*100.1*	*70.3*	*N/A*	*N/A*
1	405.6	403.5	400.4	396.6	395.5	1.1	-31.4	-35.49	30.7	1.6	40	4
0.8	324.7	322.8	320.7	318.3	317.3	0.8	-27.3	-30.4	24.8	1.2	40	12
0.6	243.1	241.5	240.2	238.8	237.9	0.6	-24.0	-26.4	20.5	1.4	40	18
0.4	162.1	160.6	160.0	159.4	158.5	0.4	-21.7	-23.6	16.4	0.3	40	23
0.2	80.5	79.2	78.9	78.7	78.0	0.2	-20.2	-21.9	13.8	-0.3	40	26
pu			(MW)					(MVar)			(MVar)	

A.1.2 100 km

Table A.1.3 and table A.1.4 has a variable power compensation in node 3 and node 4.

Table A.1.3: Complete power flow, 100 km, 50 Hz

$P_{1,\,ref}$	P_1	P_2	P_3	P_4	P_5	Q_1	Q_2	Q_3	Q_4	Q_5	$Q_{3,comp}$	$Q_{4,comp}$
1	*406.5*	*404.1*	*391.9*	*378.2*	*375.8*	*3.0*	*-33.6*	*615.7*	*850.8*	*763.3*	*N/A*	*N/A*
1	405.8	403.6	391.5	386.4	385.3	3.1	-30.7	143.7	29.0	0.7	225	220
0.8	324.8	322.8	313.2	309.4	308.4	2.4	-27.3	147.0	23.4	0.4	228	228
0.6	244.4	242.7	235.1	232.2	231.3	1.8	-24.8	146.3	19.0	0.2	232	232
0.4	161.8	160.2	154.1	152.0	151.2	1.2	-23.0	144.8	14.8	-1.0	235	235
0.2	81.9	80.5	75.3	73.6	72.8	0.6	-22.0	143.9	13.3	-0.8	236	236
pu			(MW)					(MVar)			(MVar)	

Table A.1.4: Complete power flow, 100 km, 16.7 Hz

$P_{1,\,ref}$	P_1	P_2	P_3	P_4	P_5	Q_1	Q_2	Q_3	Q_4	Q_5	$Q_{3,comp}$	$Q_{4,comp}$
1	*406.7*	*404.4*	*396.3*	*392.0*	*390.8*	*1.0*	*-32.2*	*142.5*	*217.2*	*184.6*	*N/A*	*N/A*
1	405.9	403.6	394.9	391.1	390.0	1.0	-31.7	44.9	28.2	-0.5	59	59
0.8	323.1	321.2	315.4	312.9	311.9	0.8	-27.6	44.6	22.1	-0.3	63	63
0.6	243.6	241.9	238.3	236.8	235.9	0.6	-24.4	44.3	19.0	-0.1	66	66
0.4	161.6	160.1	158.2	157.4	156.6	0.4	-22.0	44.2	16.4	0.5	68	68
0.2	80.3	78.9	78.0	77.6	76.9	0.2	-20.5	44.1	15.1	1.0	69	69
pu			(MW)					(MVar)			(MVar)	

A.1.3 200 km

A distance of 200 km would make the cable the longest HVAC cable in the world. Node 3 and node 4 has a variable reactive compensation, as shown in table A.1.5 and table A.1.6.

Table A.1.5: Complete power flow, 200 km, 50 Hz

$\mathbf{P_{1,\,ref}}$	$\mathbf{P_1}$	$\mathbf{P_2}$	$\mathbf{P_3}$	$\mathbf{P_4}$	$\mathbf{P_5}$	$\mathbf{Q_1}$	$\mathbf{Q_2}$	$\mathbf{Q_3}$	$\mathbf{Q_4}$	$\mathbf{Q_5}$	$\mathbf{Q_{3,comp}}$	$\mathbf{Q_{4,comp}}$
1	*406.2*	*402.9*	*315.4*	*256.7*	*249.7*	*3.0*	*-47.7*	*1 786*	*1 956*	*1 658*	*N/A*	*N/A*
1	405.7	403.2	340.0	334.6	333.6	3.0	-35.3	233.4	25.4	0.8	580	282
0.8	325.4	323.1	263.8	259.3	258.4	2.4	-32.7	238.3	20.8	0.7	580	290
0.6	243.4	241.3	185.3	181.6	180.8	1.8	-30.6	240.0	16.9	0.1	580	295
0.4	162.6	160.6	107.3	104.1	103.3	1.2	-29.0	238.2	16.3	1.7	580	295
0.2	80.5	78.7	27.3	24.5	23.7	0.6	-28.1	232.7	14.3	0.7	580	293
pu			(MW)					(MVar)			(MVar)	

Table A.1.6: Complete power flow, 200 km, LFAC 16.7 Hz

$\mathbf{P_{1,\,ref}}$	$\mathbf{P_1}$	$\mathbf{P_2}$	$\mathbf{P_3}$	$\mathbf{P_4}$	$\mathbf{P_5}$	$\mathbf{Q_1}$	$\mathbf{Q_2}$	$\mathbf{Q_3}$	$\mathbf{Q_4}$	$\mathbf{Q_5}$	$\mathbf{Q_{3,comp}}$	$\mathbf{Q_{4,comp}}$
1	*405.7*	*403.3*	*384.9*	*378.5*	*377.1*	*1.0*	*-33.3*	*343.5*	*419.4*	*376.6*	*N/A*	*N/A*
1	405.4	403.1	383.9	379.5	378.5	1.0	-32.3	160.2	28.6	0.8	100	135
0.8	323.7	321.7	307.7	304.8	303.8	0.8	-28.4	133.0	22.3	-0.4	121	122
0.6	243.7	241.9	232.1	230.1	229.2	0.6	-25.2	132.1	19.3	0.5	124	124
0.4	162.1	160.5	153.8	152.5	151.7	0.4	-22.7	130.9	15.7	-0.1	126	126
0.2	81.7	80.2	75.4	74.6	73.8	0.2	-21.1	129.3	12.9	-1.2	127	127
pu			(MW)					(MVar)			(MVar)	

A.1.4 300 km

Table A.1.7 is not shown below $P_{1,\,\mathrm{ref}} = 0.7$ pu as there is no active power delivered to shore, the power flow in node 5 is negative, and the system consumes active power. However, both voltage (figure A.3.1) and current (figure A.2.4) are too high for the cable to operate at 50 Hz with reactive power compensation from one side of the cable only.

Table A.1.7: Complete power flow, 300 km, 50 Hz

$\mathbf{P_{1,\,ref}}$	$\mathbf{P_1}$	$\mathbf{P_2}$	$\mathbf{P_3}$	$\mathbf{P_4}$	$\mathbf{P_5}$	$\mathbf{Q_1}$	$\mathbf{Q_2}$	$\mathbf{Q_3}$	$\mathbf{Q_4}$	$\mathbf{Q_5}$	$\mathbf{Q_{3,comp}}$	$\mathbf{Q_{4,comp}}$
1	405.4	402.0	128.7	122.3	121.5	3.0	-49.9	395.8	10.0	-5.0	1 065	400
0.8	324.2	321.0	77.69	71.7	70.9	2.3	-48.1	390.5	12.7	-1.4	1 065	395
0.7	283.8	280.6	40.5	34.8	34.0	2.0	-47.2	384.1	14.1	0.5	1 065	390
pu			(MW)					(MVar)			(MVar)	

Table A.1.8: Complete power flow, 300 km, LFAC 16.7 Hz

$P_{1,\,ref}$	P_1	P_2	P_3	P_4	P_5	Q_1	Q_2	Q_3	Q_4	Q_5	$Q_{3,comp}$	$Q_{4,comp}$
1	*406.6*	*404.0*	*368.1*	*357.3*	*355.8*	*1.0*	*-35.2*	*578.2*	*653.8*	*591.3*	*N/A*	*N/A*
1	404.7	402.2	366.3	361.8	360.7	1.0	-33.2	203.6	26.8	0.3	196	165
0.8	324.0	321.8	293.1	289.6	288.7	0.8	-29.5	207.4	24.0	2.1	196	170
0.6	242.7	240.8	217.8	215.3	214.4	0.6	-26.3	208.9	18.8	0.7	196	175
0.4	163.3	161.6	142.9	141.0	140.2	0.4	-23.9	208.1	14.2	-1.3	196	178
0.2	81.6	80.0	64.2	62.7	62.0	0.2	-22.2	204.8	11.3	-2.6	196	176
pu			(MW)					(MVar)			(MVar)	

Table A.1.9: Complete power flow, 300 km, LFAC 16.7 Hz with reactive compensation offshore

$P_{1,\,ref}$	P_1	P_2	P_3	P_4	P_5	Q_1	Q_2	Q_3	Q_4	Q_5	$Q_{2,comp}$	$Q_{3,comp}$	$Q_{4,comp}$
1	405.9	403.7	376.8	372.6	371.5	1.0	-178.9	162.7	23.8	-3.5	82	125	140
0.8	323.6	321.8	302.4	299.3	298.3	0.8	-171.8	170.3	24.7	2.3	82	125	145
0.6	243.4	241.7	228.3	226.0	225.1	0.6	-165.1	175.2	18.5	-0.1	82	125	153
0.4	162.4	161.0	152.0	150.3	149.5	0.4	-159.0	178.0	15.8	0.1	82	125	157
0.2	81.3	80.3	73.8	72.6	71.8	0.2	-153.6	178.2	11.9	-2.1	82	125	160
pu			(MW)					(MVar)				(MVar)	

A.2 Currents at Different Cable Lengths, 50 Hz and LFAC 16.7 Hz

This section shows the plot of the currents at different cable lengths.

With offshore reactive power compensation of 82 MVar in node 2, the current for a cable length of 300 km is depicted in figure A.2.5.

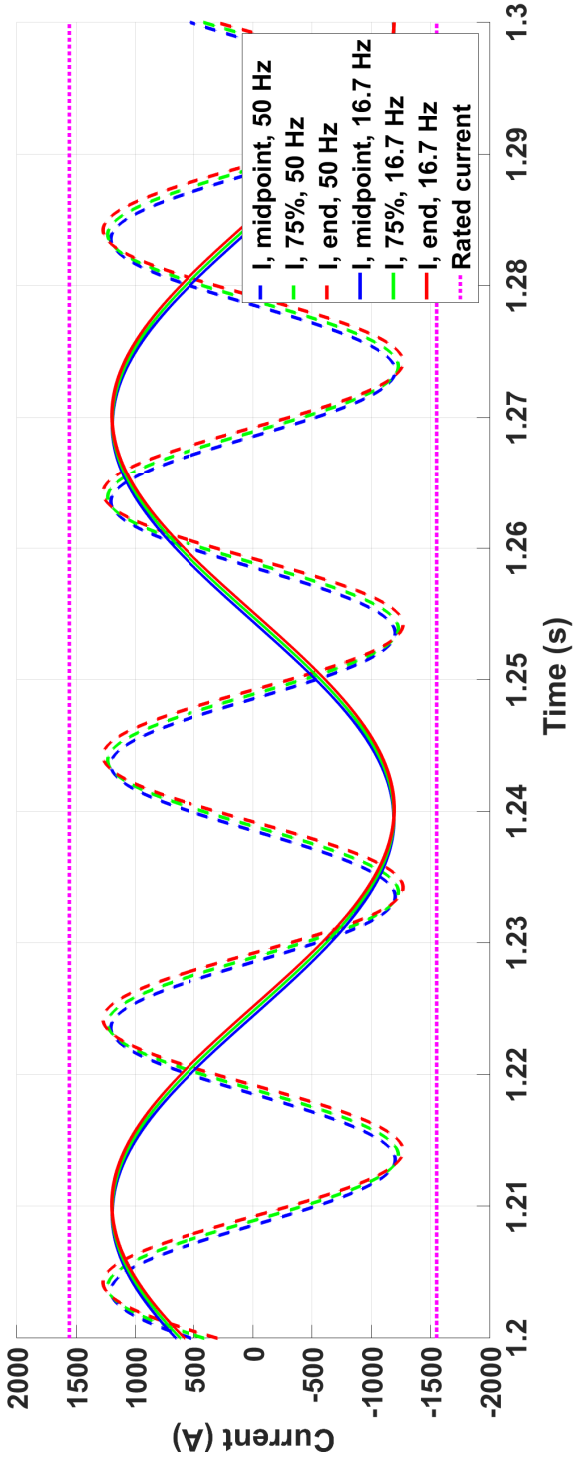

Figure A.2.1: 35 km cable current at rated power

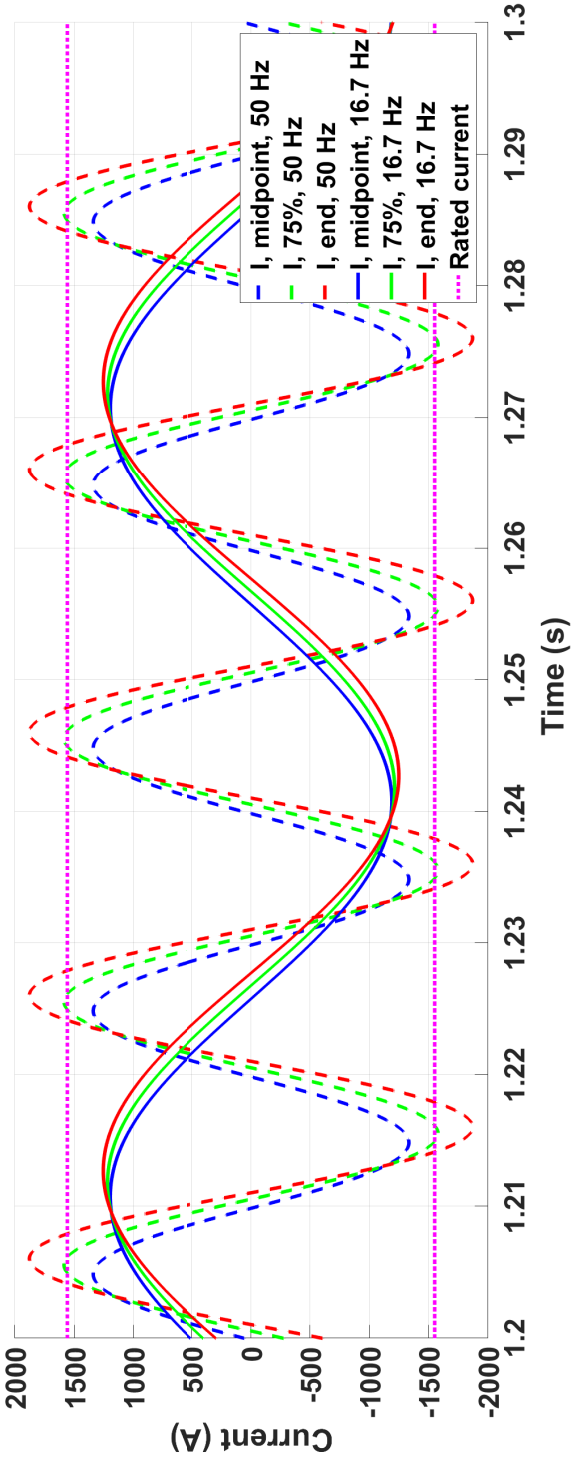

Figure A.2.2: 100 km cable current at rated power

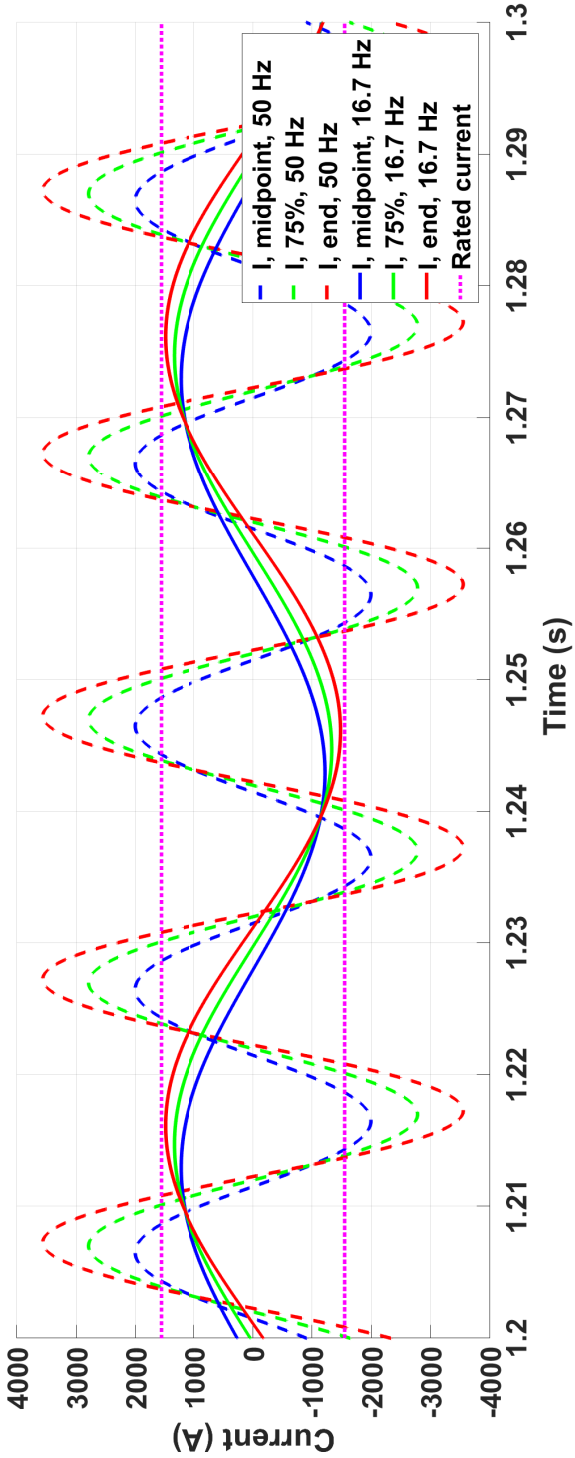

Figure A.2.3: 200 km cable current at rated power

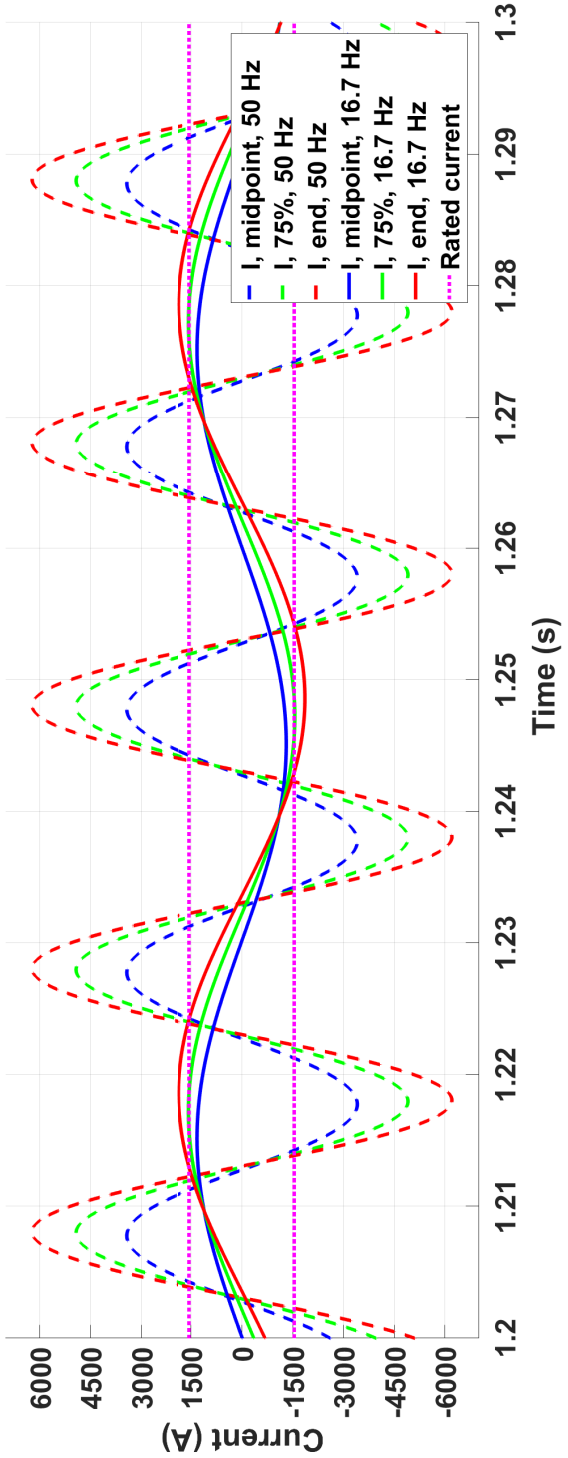

Figure A.2.4: 300 km cable current at rated power

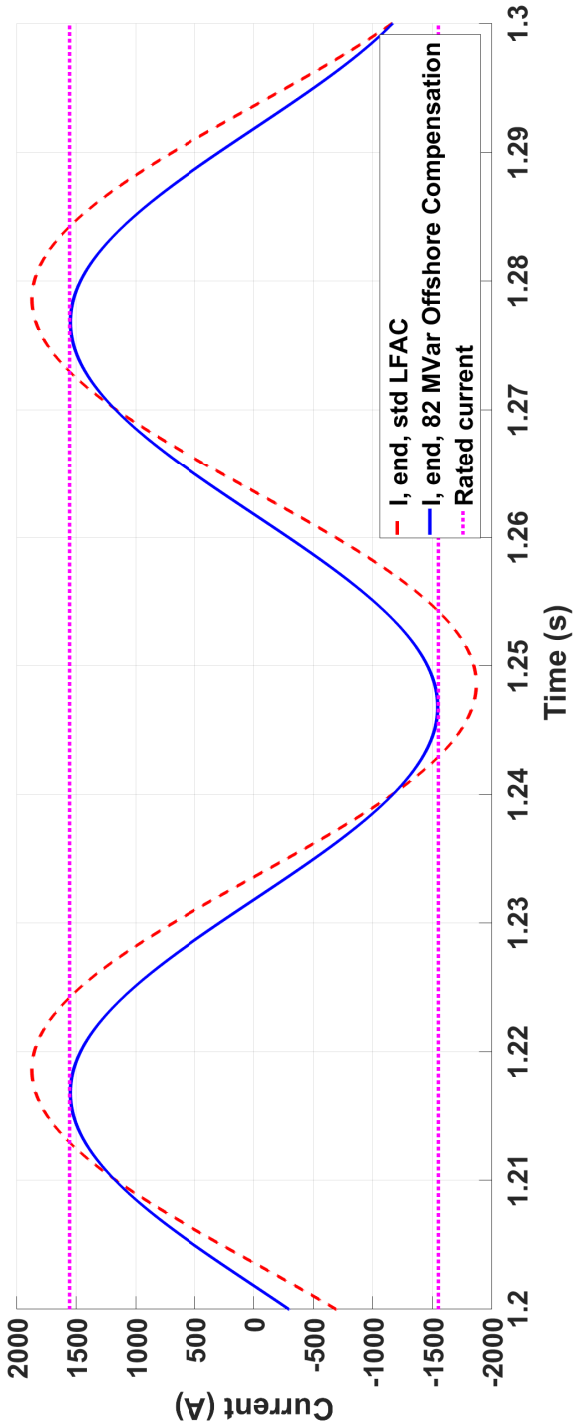

Figure A.2.5: Phase current with reactive compensation in one end (red) and in both ends (blue), 300 km, LFAC 16.7 Hz

A.3 Voltage at Different Cable Lengths, 50 Hz and LFAC 16.7 Hz

The voltages at the sending end of the cable for different cable lengths and frequencies are depicted in figure A.3.1.

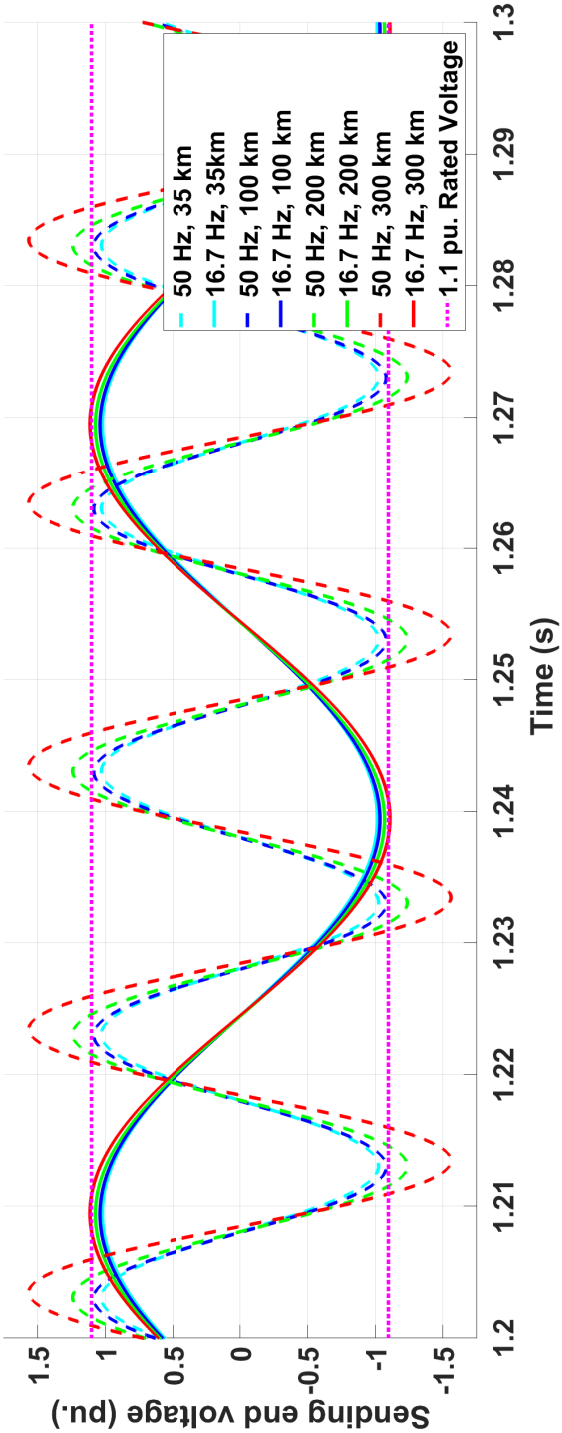

Figure A.3.1: Cable voltage at sending end, pu.

Appendix B

Type 1-4 Wind Turbine Generators

Modern WTGs are divided into four different types depending on their topology and connection to the collection grid. There is also a fifth type using a variable speed drive train connected to a torque/speed converter coupled with a synchronous generator [20].

B.1 Type 1, Fixed Speed

The turbine Type 1 has a fixed (or nearly fixed) speed that is directly proportional to the grid frequency, also making the rotational speed of the turbine blades fixed [20]. The Type 1 uses a squirrel-cage induction generator (SCIG) that is connected directly to the step up transformer in the WTG as shown in figure B.1.1a with a capacitor bank for reduction of the reactive power consumption [21]. Due to variations in the wind speed, such as gusts, the fixed speed rotation would lead to large variations in the mechanical stress on the turbine and its blades. The fixed speed turbines would also not be able to adjust the power coefficient optimally as it would only be able to adjust the pitching of the blades, and not the rotational speed. The power coefficient is a function of both the ratio between the speed at the tip of the turbine blades and wind speed, and the blade pitch, $C_p(\lambda, \beta)$, which has already been described in section 3.1. However some of the generators have two sets of windings, one used for low wind speeds with a high number of pole pairs and one used for high wind speeds with a lower number of pole pairs [21]. The simple design also include a soft starter in order to reduce the large inrush starting currents [43].

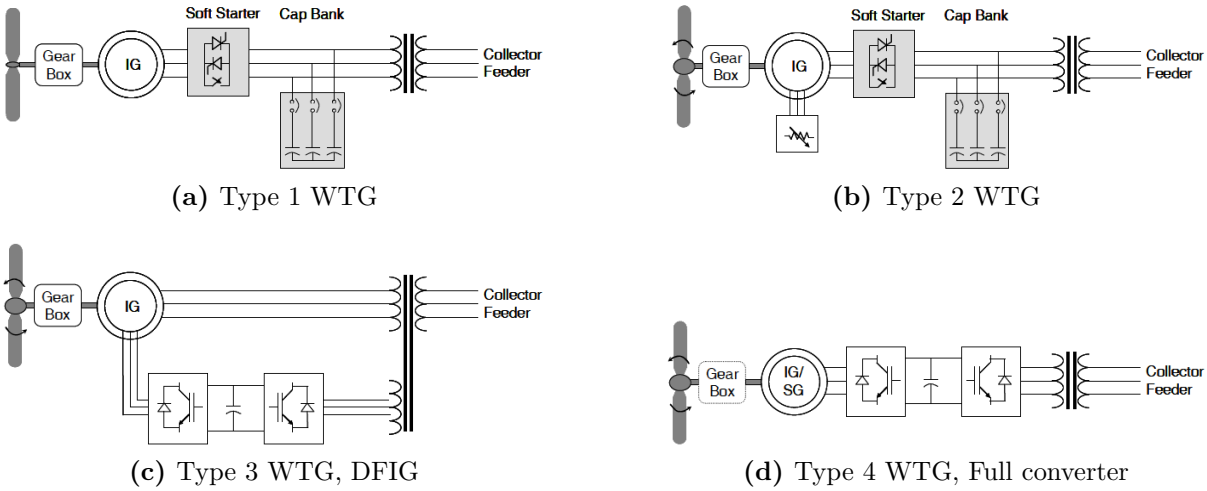

(a) Type 1 WTG

(b) Type 2 WTG

(c) Type 3 WTG, DFIG

(d) Type 4 WTG, Full converter

Figure B.1.1: Different types of generator topologies used in wind farms [20]

B.2 Type 2, Limited Variable Speed

The Type 2, shown in figure B.1.1b, is similar to type 1 in the connection of the stator circuit, however the rotor circuit is connected to a resistor of variable size [20]. The resistors are used to change the shape of the power curve of the generator so that it can operate at different speeds for the same power output [43]. An increase in rotor resistance would result in a higher speed for the same power output. The variable resistors make possible for a speed variation of up to 10 % [20], which is beneficial considering for instance tip speed ratios as mentioned in section 3.1.

B.3 Type 3, Partial Rated Power Electronic Converter

The next advance is the Type 3, also known as the *Doubly Fed Induction Generator*. The term doubly fed comes from how the generator is connected to the electrical grid. The stator is directly connected to the grid while the rotor is fed through a power electronic converter. Since only the rotor is connected through the converter it typically has a rating of approximately 30 % of the active power rating of the generator [22]. The rotor current is controlled by a voltage source converter which adjusts the phase and magnitude of the current, making the DFIG able to adjust the reactive power produced/consumed by the

generator [20]. The DFIG can typically operate ±30 % of the synchronous speed [21]. The general topology is shown in figure B.1.1c.

B.4 Type 4 Generator, Fully Rated Power Electronic Converter

The fully rated converter topology, known as Type 4, offers a great deal of flexibility when choosing a generator as it decouples the rotation of the generator from the grid using the back-to-back converter, as shown in figure B.1.1d. This allows the turbine to operate at variable speed and thus achieving the optimal C_p. The ability to control both active and reactive power flow makes this type of topology able to use any type of generator. The Type 4 WTG has been constructed with wound rotor synchronous generators, with control of the field current and a high number of generator pole-pairs, as permanent magnet synchronous generators or as squirrel cage induction generators [20]. Synchronous generators are becoming more popular and the multipole PMSGs seems to become the most adapted generator for larger WTGs (3-8 MW) in the future, however there is a risk of this not to turn out as expected as the topology could be sensitive to increased prices of the rare earth metals used in the permanent magnets [22]. The Vestas *V164-8.0 MW* uses a Type 4 Permanent Magnet Synchronous Generator (PMSG).

Appendix C

DQ-transformation

This chapter is based on the book *Advanced Electric Drives* by *Ned Mohan*, [44].

In general a three-phase AC system where the current in each of the different phases is shifted $\frac{\pi}{3}$ electrical radians and comprising of windings that are spatially oriented $\frac{\pi}{3}$ radians apart from each other. Each current sets up an electromagnetic field that is perpendicular to the plane between the sending and returning wire of each phase, according to *Ampere's Law*. The three phases results in an equivalent magnetic field with a constant magnitude of 1.5 times the amplitude of each phase signals rotating at $\omega = 2\pi f$ radians per second.

The current in winding aa' is producing a perpendicular magnetic field with sinusoidally varying magnitude. This is also the case for bb' and cc' except being delayed by $\frac{\pi}{3}$ electrical radians. Superposition of the contributions from each phase gives a rotating net magnetic field of 1.5 times the amplitude of magnetic density of each phase, as shown in equation C.0.4 and figure C.0.1.

$$B_{aa'}(t) = \hat{B}\sin(wt) \tag{C.0.1}$$

$$B_{bb'}(t) = \hat{B}\sin(wt - \frac{2\pi}{3})\angle\frac{2\pi}{3} \tag{C.0.2}$$

$$B_{cc'}(t) = \hat{B}\sin(wt - \frac{4\pi}{3})\angle\frac{4\pi}{3} \tag{C.0.3}$$

$$B(t) = B_{aa'}(t) + B_{bb'}(t) + B_{cc'}(t) = 1.5\hat{B}\angle(wt - \frac{\pi}{2}) \tag{C.0.4}$$

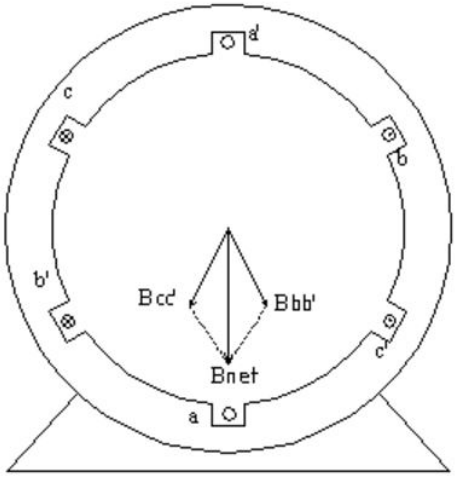

Figure C.0.1: Magnetic field contributions at $wt = 0$

C.1 Park's transformation [44]

In order to use control systems to adjust the voltage and currents of the circuit it is beneficial to express the voltages and currents in a reference system so that they appear to have a constant value. This is done using the *Park transformation*, changing the reference from a static abc-reference frame, to a rotating dq-reference frame, at a speed of ω radians per second. For dynamic control and analysis of AC-machines, the three phase circuit must be expressed in two orthogonal windings making independent control of both the magnetic flux and torque of the machine possible. For a three phase system the resulting magnetomotive force space vector is made from the current space vector of each phase.

$$\vec{i}_s^a(t) = i_a(t) + i_b(t)e^{j\frac{2\pi}{3}} + i_c(t)e^{j\frac{4\pi}{3}} \tag{C.1.1}$$

For any given time the d- and q-axis windings can produce the equivalent magnetic field in the machine as a three phase system.

$$\vec{F}_s^a(t) = \frac{N_s}{p}\vec{i}_s^a(t) \tag{C.1.2}$$

The magnetomotive force (mmf) space vector $\vec{F}_s(t)$ relates to $\vec{i}_s(t)$ by a factor of $(\frac{N_s}{p})$ where p is the number of poles and N_s is the number of turns per phase, see eqution C.1.2.

Given that the dq-axis representation must produce the same mmf as the three phase system the relationship between the two, referred to the d-axis is given by equation C.1.3, and the result can be seen in figure C.0.1 where the projections are shown.

$$(i_{sd} + ji_{sq}) = \sqrt{\frac{2}{3}}\vec{i}_s^d \tag{C.1.3}$$

Figure C.1.1 shows the different axes at an arbitrary time t. The d- and q-axis rotate at the same speed as the resulting stator current space vector $\vec{i}_s(t)$, rotating at ω electrical radians per second.

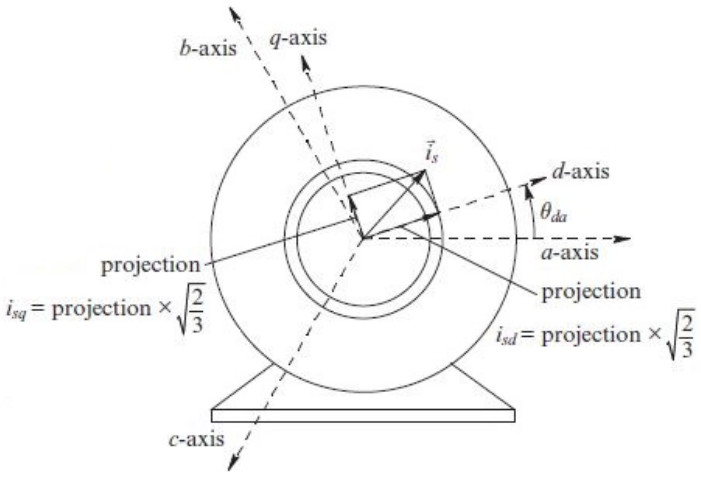

Figure C.1.1: Stator dq-axes [44]

Combining equation (C.1.1) and (C.1.3) gives the Park' Transformation from the abc-reference frame to the dq-reference frame. θ_{da} in equation (C.1.4) refers to the angle between the stator a-axis and the rotating d-axis.

$$\begin{bmatrix} i_{sd}(t) \\ i_{sd}(t) \end{bmatrix} = \sqrt{\frac{2}{3}} \begin{bmatrix} \cos(\theta_{da}) & \cos(\theta_{da} - \frac{2\pi}{3}) & \cos(\theta_{da} - \frac{4\pi}{3}) \\ \sin(\theta_{da}) & -\sin(\theta_{da} - \frac{2\pi}{3}) & -\sin(\theta_{da} - \frac{4\pi}{3}) \end{bmatrix} \begin{bmatrix} i_a(t) \\ i_b(t) \\ i_c(t) \end{bmatrix} \tag{C.1.4}$$

Bibliography

[1] United Nations, Department of Economic and Social Affairs, "The 2015 revision of the UN's world population projections," *Population and Development Review*, vol. 41, pp. 557–561, sep 2015.

[2] OECD, "Technology roadmap wind energy 2013," tech. rep., OECD, 2013.

[3] Teknisk Ukeblad, "Statoil vil bruke Hywind til å levere strøm til Kvitebjørn og Valemon." `http://www.tu.no/petroleum/2015/11/26/statoil-vil-bruke-hywind-til-a-levere-strom-til-kvitebjorn-og-valemon`, November 2015. (Visited on 12/10/2015).

[4] M. Hirth, "Anbefaler at Statoil får flytte Hywind til oljeplattformer." `http://sysla.no/gronn/anbefaler-at-statoil-far-flytte-hywind-til-oljeplattformer/`, Apr. 2016. (Visited on 04/03/2017).

[5] Teknisk Ukeblad, "Statoil dropper å flytte Hywind-demoen til Valemon." `https://www.tu.no/live/79318`. (Visited on 14/04/2017).

[6] Statoil, "Statoil to build the world's first floating wind farm: Hywind Scotland." `https://www.statoil.com/en/news/hywindscotland.html`, Nov. 2015. (Visited on 20/01/2017).

[7] OECD, "Medium-term renewable energy market report 2015," tech. rep., OECD, oct 2015.

[8] OECD, "Medium-term renewable energy market report 2016," tech. rep., OECD, oct 2016.

[9] IRENA, The International Renewable Energy Agency, "Renewable capacity statistics 2017," 2017.

[10] E. Thibaut and B. Leforgeais, "Selection of power from shore for an offshore oil and gas development," *IEEE Transactions on Industry Applications*, vol. 51, pp. 1333–1340, March 2015.

[11] K. Allgot, "Low Frequency AC Transmission for Offshore Wind Farms." Specialization Project Report at the Norwegian University of Science and Technology (NTNU), Dec. 2015.

[12] Vattenfall AB, "HORNS REV 3 OFFSHORE WIND FARM." `https://corporate.vattenfall.com/about-energy/renewable-energy-sources/wind-power/wind-power-at-vattenfall/horns-rev-3-offshore-wind-farm/`, June 2016. (Visited on 08/02/2017).

[13] MHI Vestas, "World's most powerful wind turbine once again smashes 24 hour power generation record as 9 mw wind turbine is launched." `http://www.mhivestasoffshore.com/new-24-hour-record/`, Jan. 2017. (Visited on 14/02/2017).

[14] Energinet DK, "Technical project description for the large-scale offshore wind farm (400 mw) at horns rev 3," in *Horns Rev 3*, no. 244257/13, Oct 2013.

[15] PhD. C. F. Jensen, Energinett, "Horns Rev 3, cable data, grid connection and reactive power compensation." Personal communication, Apr. 2017. Interview.

[16] 4C Offshore, "Horns rev 3 substation." `http://www.4coffshore.com/windfarms/substation-horns-rev-3-substation-sid338.html`, 2017. (Visited on 11/03/2017).

[17] H. Brantsæter, "Harmonic Resonance Mode Analysis and Application for Offshore Wind Power Plants," Master's thesis, Norwegian University of Science and Technology, NTNU, Dec. 2015.

[18] Energinet DK, *Technical regulation 3.2.5 for wind power plants above 11 kW*, 4.1 ed., July 2016.

[19] J. Manwell, J. McGowan, and A. Rogers, *Wind energy explained: theory, design and application*. John Wiley & Sons, 2010.

[20] E. Camm, M. Behnke, O. Bolado, M. Bollen, M. Bradt, C. Brooks, W. Dilling, M. Edds, W. Hejdak, D. Houseman, S. Klein, F. Li, J. Li, P. Maibach, T. Nicolai,

J. Patino, S. Pasupulati, N. Samaan, S. Saylors, T. Siebert, T. Smith, M. Starke, and R. Walling, "Characteristics of wind turbine generators for wind power plants," in *Power Energy Society General Meeting, 2009. PES '09. IEEE*, pp. 1–5, July 2009.

[21] A. Hansen, F. Iov, F. Blaabjerg, and L. Hansen, "Review of Contemporary Wind Turbine Concepts and their Market Penetration," *Journal of Wind Engineering & Industrial Aerodynamics*, vol. 28, no. 3, pp. 247–263, 2004.

[22] F. Blaabjerg, M. Liserre, and K. Ma, "Power Electronics Converters for Wind Turbine Systems," *Industry Applications, IEEE Transactions on*, vol. 48, pp. 708–719, March 2012.

[23] I. Erlich, F. Shewarega, H. Wrede, and W. Fischer, "Low frequency AC for offshore wind power transmission - prospects and challenges," in *AC and DC Power Transmission, 11th IET International Conference on*, pp. 1–7, Feb 2015.

[24] ABB, "Why HVDC Economic and environmental advantages - Why choose HVDC over HVAC (HVDC) | ABB." `http://new.abb.com/systems/hvdc/why-hvdc/economic-and-environmental-advantages`, 2015. (Visited on 12/07/2015).

[25] F. Li, P. Yang, Q. Zheng, S. Zhou, and Q. Wang, "Research on reactive power compensation optimization design based on equivalent model of offshore wind farm," in *Power and Energy Engineering Conference (APPEEC), 2014 IEEE PES Asia-Pacific*, pp. 1–6, Dec 2014.

[26] M. Jafar and M. Molinas, "A Transformerless Series Reactive/Harmonic Compensator for Line-Commutated HVDC for Grid Integration of Offshore Wind Power," *Industrial Electronics, IEEE Transactions on*, vol. 60, pp. 2410–2419, June 2013.

[27] The MathWorks Inc., *MATLAB/Simulink/SimPowerSystems*, R2016b ed., 2016.

[28] J. Ruddy, R. Meere, and T. O'Donnell, "Low Frequency AC transmission as an alternative to VSC-HVDC for grid interconnection of offshore wind," in *PowerTech, 2015 IEEE Eindhoven*, pp. 1–6, June 2015.

[29] Erlich, I. and Shewarega, F. and Feltes, C. and Koch, F.W. and Fortmann, J., "Offshore Wind Power Generation Technologies," *Proceedings of the IEEE*, vol. 101, pp. 891–905, April 2013.

[30] H. Chen, M. Johnson, and D. Aliprantis, "Low-Frequency AC Transmission for Offshore Wind Power," *Power Delivery, IEEE Transactions on*, vol. 28, pp. 2236–2244, Oct 2013.

[31] W. Fischer, R. Braun, and I. Erlich, "Low frequency high voltage offshore grid for transmission of renewable power," in *Innovative Smart Grid Technologies (ISGT Europe), 2012 3rd IEEE PES International Conference and Exhibition on*, pp. 1–6, Oct 2012.

[32] T. Funaki and K. Matsuura, "Feasibility of the low frequency AC transmission," in *Power Engineering Society Winter Meeting, 2000. IEEE*, vol. 4, pp. 2693–2698 vol.4, 2000.

[33] N. Qin, S. You, Z. Xu, and V. Akhmatov, "Offshore wind farm connection with low frequency AC transmission technology," in *Power Energy Society General Meeting, 2009. PES '09. IEEE*, pp. 1–8, July 2009.

[34] ABB, "XLPE Submarine Cable Systems." Brochure, 2010.

[35] European Electricity Grid Initiative, "E-Highway2050, WP3 workshop April 15th, 2014 Brussels." `http://www.e-highway2050.eu/fileadmin/documents/Workshop4/7b_Europacable_for_WP3_Workshop_Technology_Presentation_15_April_2014_c.pdf`, 2014. (Visited on 25/01/2017).

[36] P. Wyllie, Y. Tang, L. Ran, T. Yang, and J. Yu, "Low Frequency AC Transmission - Elements of a Design for Wind Farm Connection," in *AC and DC Power Transmission, 11th IET International Conference on*, pp. 1–5, Feb 2015.

[37] A. Canelhas, S. Karamitsos, U. Axelsson, and E. Olsen, "A low frequency power collector alternative system for long cable offshore wind generation," in *AC and DC Power Transmission, 11th IET International Conference on*, pp. 1–6, Feb 2015.

[38] S. Sanchez, *Stability Investigation of Power Electronics Systems - A Microgrid Case*. PhD thesis, Norwegian University of Science and Technology (NTNU), Mar. 2015.

[39] International Electrotechnical Commission, *IEC62067:2011. Power cables with extruded insulation and their accessories for rated voltages above 150 kV (Um=170 kV) up to 500 kV (Um=550 kV) - Test methods and requirements*, Nov. 2011.

[40] M. Santos-Mugica, E. Robles, A. G. Endegnanew, E. Tedeschi, and J. Giebhardt, "Grid integration and power quality testing of Marine Energy Converters: Research activities in the MaRINET Project," in *2014 Ninth International Conference on Ecological Vehicles and Renewable Energies (EVER)*, pp. 1–9, March 2014.

[41] Esa Virtanen, Vice President, ABB Transformers, "Questions regarding low frequency AC operation of sentral power system components in an offshore wind farm.." Personal communication, June 2017. Interview.

[42] T. K. Vrana and O. Mo, "Optimal Operation Voltage for Maximal Power Transfer Capability on Very Long HVAC Cables," *Energy Procedia*, vol. 94, pp. 399–408, Jan. 2016.

[43] S. Chapman, *Electric Machinery Fundamentals*. Tata McGraw-Hill Education, 5th ed., 2005.

[44] N. Mohan, *Advanced Electric Drives: Analysis, Control, and Modeling Using MATLAB/Simulink*. JOHN WILEY & SONS INC, July 2014.